Generation of functional human thymic cells from induced pluripotent stem cells

Stephan A. Ramos, BS,[a] John J. Morton, PhD,[b] Prabha Yadav, MBA,[a] Brendan Reed, PhD,[a,c] Sheila I. Alizadeh,[a] Ali H. Shilleh, MSc,[a] Loni Perrenoud, BS,[b] James Jaggers, MD,[f] John Kappler, PhD,[a,e] Antonio Jimeno, MD, PhD,[b,d] and Holger A. Russ, PhD[a,d]* *Aurora and Denver, Colo*

Background: The thymus is a glandular organ that is essential for the formation of the adaptive immune system by educating developing T cells. The thymus is most active during childhood and involutes around the time of adolescence, resulting in a severe reduction or absence of naive T-cell output. The ability to generate a patient-derived human thymus would provide an attractive research platform and enable the development of novel cell therapies.

Objectives: This study sought to systematically evaluate signaling pathways to develop a refined direct differentiation protocol that generates patient-derived thymic epithelial progenitor cells from multiple induced pluripotent stem cells (iPSCs) that can further differentiate into functional patient-derived thymic epithelial cells on transplantation into athymic nude mice.

Methods: Directed differentiation of iPSC generated TEPs that were transplanted into nude mice. Between 14 and 19 weeks posttransplantation, grafts were removed and analyzed by flow cytometry, quantitative PCR, bulk RNA sequencing, and single-cell RNA sequencing for markers of thymic-cell and T-cell development.

Results: A direct differentiation protocol that allows the generation of patient-derived thymic epithelial progenitor cells from multiple iPSC lines is described. On transplantation into athymic nude mice, patient-derived thymic epithelial progenitor cells further differentiate into functional patient-derived thymic epithelial cells that can facilitate the development of T cells. Single-cell RNA sequencing analysis of iPSC-derived grafts shows characteristic thymic subpopulations and patient-derived thymic epithelial cell populations that are indistinguishable from TECs present in primary neonatal thymus tissue.

Conclusions: These findings provide important insights and resources for researchers focusing on human thymus biology. (J Allergy Clin Immunol 2021;■■■:■■■-■■■.)

Key words: *Human neonatal thymus, patient derived induced pluripotent stem cells, direct differentiation, thymic epithelial progenitors, thymic epithelial cells, single-cell RNA sequencing*

The thymus is a glandular organ that is essential for the generation of a functional adaptive immune system by providing positive and negative selection of developing T cells.[1] The thymus is an endodermal-derived tissue and originates from the third pharyngeal pouch (TPP) during embryonic development.[2] Thymic epithelial progenitor cells (TEPs) in the TPP can be identified by the expression of the master transcription factor Foxn1 marking the thymic anlage that is surrounded by supporting mesenchymal cells. Foxn1 is necessary for the development of thymic epithelial cells (TECs) and, subsequently, a functional thymus. In both mice and humans, disruption of FOXN1 causes congenital athymia.[3,4] Loss of Foxn1 in the adult thymus results in thymic atrophy, similar to that observed in aged individuals.[5,6] While the specification of TEPs is independent of Foxn1 expression, Foxn1 is required for the differentiation of functional TECs from TEPs.[7] Additionally, differentiation of TEPs into functional TECs depends on interaction with developing T cells.[8-10] Functional TECs can be divided into 2 distinct subtypes based on their location and function—cortical and medullary TECs (cTECs and mTECs, respectively)—and can be identified by the expression of cytokeratin 8 and 5, respectively. Both TEC subtypes originate from a common bipotent TEC

From [a]the Barbara Davis Center for Diabetes, University of Colorado Anschutz Medical Campus, Aurora; [b]the Division of Medical Oncology, Department of Medicine, [c]the Department of Immunology and Microbiology, [d]the Charles C. Gates Center for Regenerative Medicine, and [f]the Surgery-Cardiothoracic Department, University of Colorado School of Medicine, Aurora; and [e]the Department of Biomedical Research, National Jewish Health, Denver.

*Lead author.

Supported by the National Institutes of Health (NIH): "Pre-doctoral Training in Molecular Biology" grant NIH-T32-GM008730 (to S.A.R.), "Pre-doctoral Training in Stem Cell Biology" grant NIH-T32-AR0007411-35 (to A.H.S.) and "Predoctoral training in Diabetes/Bioengineering" grant NIH-T32-DK120520-01A1 (to A.H.S.). Work in the laboratory of H.A.R. is supported by the Children's Diabetes Foundation, National Institute of Diabetes and Digestive and Kidney Diseases (NIDDK) grant R01DK120444 and National Institute of Allergy and Infectious Diseases grant R21AI140044, a new investigator award from the NIDDK-supported Human Islets Research Network (grant RRID:SCR_014393; UC24 DK1041162), the Culshaw Junior Investigator Award in Diabetes, a University of Colorado Grubstake award, and the Juvenile Diabetes Research Foundation (grant 2-SRA-2019-781-SB). Work in the laboratory of A.J. is supported by NIH grants R01CA149456 and R01CA213102, the Daniel and Janet Mordecai Foundation, the Karsh Family Foundation, and the Peter and Rhonda Grant Foundation, as well by as anonymous donors. This work was supported by NIDDK grant P30-DK116073 to the University of Colorado Diabetes Research Center.

Disclosure of potential conflict of interest: S.A. Ramos, J.J. Morton, A. Jimeno, and H.A. Russ filed patent applications based on the results presented in this work. A. Jimeno is a consultant and owns stock options in SuviCa; and owns stock in Champions Oncology. H.A. Russ is a consultant to Sigilon Therapeutics and Eli Lilly; and Scientific Advisory Board member of Prellis Biologics. The rest of the authors declare that they have no relevant conflicts of interest.

Received for publication January 20, 2021; revised June 29, 2021; accepted for publication July 1, 2021.

Corresponding author: Holger A. Russ, PhD, Barbara Davis Center for Diabetes, University of Colorado, Anschutz Medical Campus, 1775 Aurora Court, M20-4202G, Aurora, CO 80045. E-mail: holger.russ@cuanschutz.edu. Or: Antonio Jimeno, MD, PhD, University of Colorado Cancer Center and Charles C. Gates Center of Stem Cell Biology, Anschutz Medical Campus, 12801 East 17th Avenue, RC1S L18-8111, Aurora, CO 80045. E-mail: antonio.jimeno@cuanschutz.edu.

0091-6749/$36.00

https://doi.org/10.1016/j.jaci.2021.07.021

Abbreviations used
cTEC: Cortical thymic epithelial cell
d0: Day 0
DAPI: 4′-6-Diamidino-2-phenylindole, dihydrochloride
ETOH: Ethyl alcohol
hESC: Human embryonic stem cell
IF: Immunofluorescence
iPSC: Induced pluripotent stem cell
mTEC: Medullary thymic epithelial cell
qPCR: Quantitative PCR
RT: Room temperature
scRNAseq: Single-cell RNA sequencing
TEC: Thymic epithelial cell
TEP: Thymic epithelial progenitor cell
TPP: Third pharyngeal pouch
tSNE: t-Stochastic neighbor embedding

progenitor marked by coexpression of both keratins, as reviewed in Perniola.[11] Developing T cells, marked by coexpression of CD4 and CD8, are first positively selected for successful interaction with the self-peptide–bearing HLA complex proteins on cTECs before migrating into the thymic medulla as single positive CD4 or CD8 T cells.[12] This process is termed positive selection and only T cells that strongly interact with HLA/peptide receive a survival signal while the majority of developing T cells undergo death by neglect. In the thymic medulla, mTECs are essential in the establishment of central immune tolerance through the process of negative selection by presenting self-antigens to positively selected T cells. Autoreactive T cells that interact with self-antigens too strongly are eliminated, while nonreactive, functional T cells emigrate into the periphery. AIRE has been shown to be critical for regulating the expression of tissue restricted antigens in mTECs, and absence of AIRE or otherwise altered negative selection results in the development of autoimmune diseases, such as autoimmune polyendocrinopathy-candidiasis-ectodermal dystrophy.[13] While the thymus is very active in young individuals, the organ starts to involute around the age of adolescence and naive T-cell output declines rapidly.[14] Thymic involution is accelerated by certain clinical treatments, including chemotherapy.[15] In addition, congenital disease conditions impairing thymus function, including DiGeorge and severe combined immune deficiency, highlight the critical role of this organ. The ability to generate a patient-specific human thymus would provide an attractive platform to investigate human thymus biology and stimulate the development of novel treatment modalities, including cell replacement therapy.

Previously, we and others, have demonstrated the ability to generate TEPs by directed differentiation of human embryonic stem cells (hESCs).[16,17] While some recent reports have shown promise in generating TEPs from induced pluripotent stem cells (iPSCs),[18,19] differentiation conditions were either not evaluated using multiple iPSC lines or relied on transgene expression, complicating their potential use in humans. Building on previous findings, we used systematic evaluation of signaling pathway manipulation to develop a refined direct differentiation protocol that generates patient-derived TEPs from multiple iPSCs. Patient-derived TEPs can further differentiate into functional TECs on transplantation into athymic nude mice and facilitate the education of developing T cells. Single-cell RNA sequencing (scRNAseq) analysis of iPSC-derived grafts shows characteristic thymic subpopulations and TEC populations within grafts are similar to TECs present in primary neonatal thymus tissue. Taken together, we anticipate that our work provides a critical platform for the development of innovative technologies and capabilities to investigate and model thymic function in a patient-specific manner and provide novel treatment modalities in the near future.

METHODS

Cell culture

Undifferentiated iPSCs were maintained on Matrigel (Corning, Corning, NY) in mTeSR1 (Stemcell Technologies, Vancouver, British Columbia, Canada), NutriStem (Biological Industries, Cromwell, Conn), or mTeSR plus (Stemcell Technologies), as per manufacture directions. For differentiation, iPSCs were plated on Matrigel at 3.15×10^5 cells/cm^2. Differentiations were initiated 24 hours after plating and were carried out in X-VIVO10 (Lonza 04-743Q; Thermo Fisher Scientific, Waltham, Mass). Factors were added at the following concentrations: activin A, 100 ng/mL (days [d] 0-4); Wnt3a, 50 ng/mL (d0 and d9-13); TTNPB (RAR agonist), 6 nmol/L (d4-13); BMP4, 20 ng/mL (d5-13); LY364947, 5 μmol/L (d5-13); FGF8b or FGF8a, 50 ng/mL (d9-13); SAG, 100 ng/mL (d5-8); SANT-1, 0.25 μmol/L (d9-13) insulin-transferrin-selenium, 1:5000 (d0) or 1:2000 (d1-4). Number of days reflect times used for condition 4, timing of factors may differ for other conditions as per Fig 1, *B*. The following supplements were added from d9 on for differentiations used in Fig 1, *G*: Trolox, 0.1 mmol/L; heparin, 10 μg/mL; 2-phospho-L-ascorbic acid trisodium salt, 50 μg/mL; hydrocortisone 0.5 μg/mL; insulin-transferrin-selenium, 1:2000; nonessential amino acids, 1×; EGF, 20 ng/mL. To compare our protocol against previously published protocols, cells were differentiated as described for conditions 4, or as described in Parent et al[16] and Sun et al.[17] Protocols were followed as described,[17] with 1 exception. We were unable to dissociate and replate cells as described, thus differentiation was continued as monolayers without replating at d3. Supplements and factors were from Stemcell Technologies (activin A, SAG, TTNPB), R&D Systems (BMP4 and FGF8; Minneapolis, Minn), Novus Biologicals (Wnt3a; Littleton, Colo), PeproTech (FGF8a and FGF8b; Rocky Hill, NJ), VWR (TTNPB and LY364947; Radnor, Pa), Selleck Chemicals (SANT-1; Houston, Tex), Gibco (ITS and NEAA; Thermo Fisher Scientific), Sigma-Aldrich (2-phospho-L-ascorbic acid trisodium salt, heparin, hydrocortisone; St Louis, Mo), Millipore-Sigma (Trolox; Burlington, Mass). For NOTCH experiments, iPSCs were differentiated to TEPs using condition 4 and treated with gamma-secretase inhibitor (XXi) 1 μmol/L (AsisChem; Waltham, Mass).

Collection and reprogramming of PBMCS to iPSC and collection of neonatal thymus tissue

Deidentified cord blood was obtained from the University of Colorado cord blood bank (http://www.clinimmune.com/cordbloodbank/). The use of human subjects for PBMC collection was approved by the Colorado Multiple Institutional Review Board (COMIRB #14-0842; principal investigator A.J.). Human PBMCs were expanded for 6 days in StemSpan SFEM II media with Erythroid Expansion Supplement (StemCell Technologies). Erythroid progenitor cells were transduced with Okita factors using P3 Primary Cell 4D Nucleofector X Kit L (Lonza; Thermo Fisher Scientific) as described previously.[20] Transduced cells were plated on a Matrigel-coated 6-well plate and cultured in ReproTeSR Media (StemCell Technologies) for 14 days with media changes every other day. Thereafter, cultures were fed with mTESR1 (StemCell Technologies) with daily media changes. Individual iPSC colonies were picked between d12 and d18, following expansion and phenotypical analysis as outlined above. Deidentified human neonatal thymus tissue was obtained after review and approval by the Colorado Multiple Institutional Review Board as not human subject research (COMIRB #18-0347; principal investigator H.A.R.).

Quantitative real-time PCR

RNA was extracted from human pluripotent stem cell and TEP cultures and dissected grafts using a RNeasy Micro Kit (QIAGEN, Hilden, Germany) per

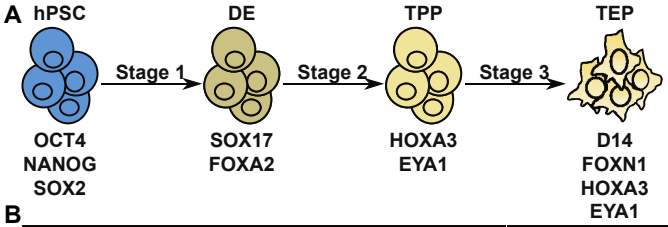

B

Conditions	Stage 1	Stage 2	Stage 3
1	Wnt3a d0; ActA d0-4; RA d4	BMP4, RA, LY d5-6	BMP4, RA, LY, Wnt3a, FGF8, SANT1
2	Wnt3a d0; ActA d0-5; RA d5	BMP4, RA, LY 6-7	BMP4, RA, LY, Wnt3a, FGF8, SANT1
3	Wnt3a d0; ActA d0-4; RA d4	BMP4, RA, LY, SAG d5-6	BMP4, RA, LY, Wnt3a, FGF8, SANT1
4	Wnt3a d0; ActA d0-4; RA d4	BMP4, RA, LY, SAG d5-8	BMP4, RA, LY, Wnt3a, FGF8, SANT1
5	Wnt3a d0; ActA d0-5; RA d5	BMP4, RA, LY, SAG d6-7	BMP4, RA, LY, Wnt3a, FGF8, SANT1
6	Wnt3a d0; ActA d0-5; RA d5	BMP4, RA, LY, SAG d6-9	BMP4, RA, LY, Wnt3a, FGF8, SANT1

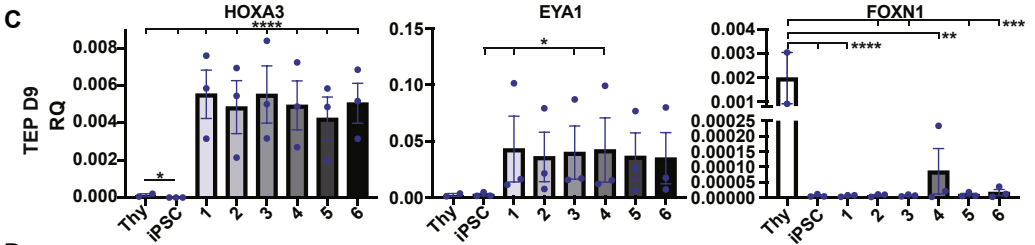

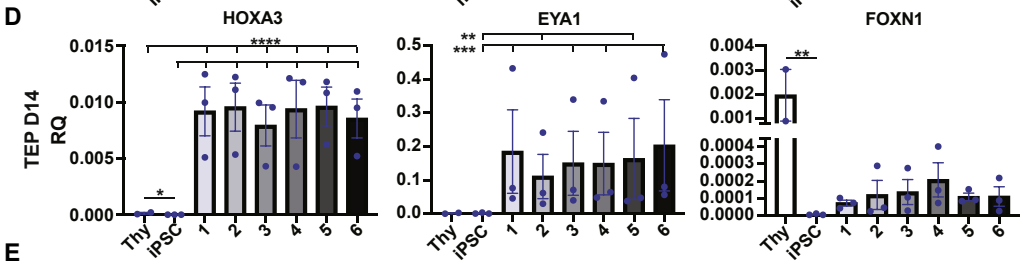

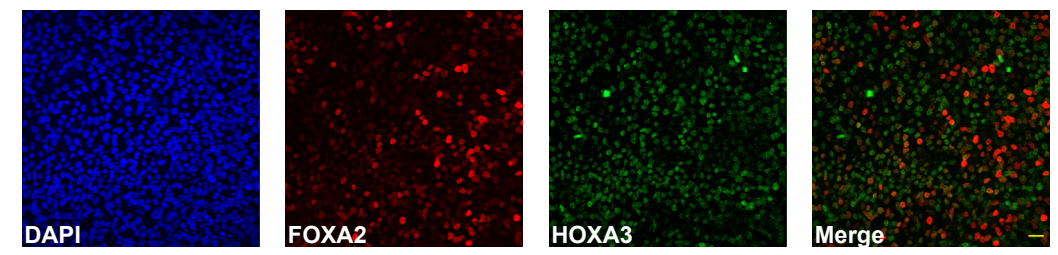

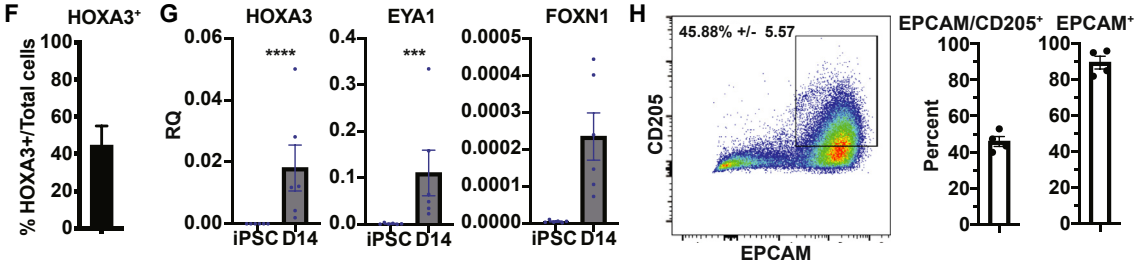

FIG 1. Generation of directed differentiation protocol for TEPs from iPSCs. **(A)** Direct differentiation approach to generate TEPs from iPSCs. **(B)** Differentiation conditions tested. qPCR analysis for TPP and TEP markers at d9 **(C)** and d14 **(D)** (n = 3, 2 iPSC lines, n = 2 primary human thymi). **(E)** Representative IF staining for endoderm marker FOXA2 (*red*) and TPP marker HOXA3 (*green*) protein at d9. Scale bar = 20 μm. **(F)** Quantification of HOXA3-positive cells over total DAPI^{+} cells. Error bars = SEM (n = 3, 3 iPSC lines). **(G)** qPCR analysis of TPP and TEP markers at d14 of TEP differentiations with condition 4 (n = 6, 4 iPSC lines). **(H)** Flow plot and bar graph quantification for EPCAM/CD205 double-positive TEPs, and EPCAM-positive cells at d14 of TEP differentiation (n = 4, 4 cell lines). qPCR values shown are relative quantification (*RQ*) to endogenous control, ACTB. *P* values of ΔΔCt values: **(C)** HOXA3: ****$P < .0001$. EYA1: *$P < .046$. **(D)** HOXA3: *$P = .034$, and **** signifies significance between primary thymus and all 6 conditions and between d0 iPSC and all 6 samples with $P \leq .0001$. EYA1: ***$P < .001$, **$P < .002$. FOXN1: $P = .0024$. **(G)** HOXA3: $P < .0001$. EYA1: $P = .0001$. *DE*, Definitive endoderm; *hPSC*, human pluripotent stem cell.

manufacturer's instructions. Reverse transcription of RNA was performed using iScript cDNA synthesis kit (1708891BUN; Bio-Rad, Hercules, Calif), as per manufacturer's instructions. Real-time quantitative PCR was performed on a CFX96 Touch Real-Time PCR Detection System (Bio-Rad) using human-specific TaqMan probes (Bio-Rad or Thermo Fisher Scientific) or human-specific primers as listed in Tables I and II, respectively. Samples were normalized to endogenous control gene *ACTB* and plotted relative to *ACTB*.

Immunofluorescence

iPSCs were cultured on hESC-grade Matrigel-coated coverslips in 24-well plates. Cultures were fixed at room temperature (RT) for 15 minutes in PBS + 4% paraformaldehyde, washed 3× with PBS, and blocked/permeabilized for 30 minutes at RT in CAS-block (Invitrogen; Thermo Fisher Scientific) + 0.2% Triton X-100. Primary antibodies (listed below) were diluted in CAS-block + 0.2% Triton X-100, and samples were stained for 1 hour at RT. Slides were washed with PBS + 0.1% Tween 3× for 5 minutes and incubated with secondary antibodies (Alexa Fluor–tagged secondary antibodies [Invitrogen]) diluted 1:1000 in PBS + 0.1% Tween and stained for 40 minutes at RT. Slides were washed 3×in PBS + 0.1% Tween and once in PBS and then were mounted in ProLong Gold antifade reagent with 4′-6-diamidino-2-phenylindole, dihydrochloride (DAPI) (Invitrogen). For tissue sections, 4- to 10-μm sections were cut from paraffin or optical cutting temperature medium–embedded tissue blocks using a microtome or cryostat, respectively, and placed on microscope slides. Deparaffination and antigen retrieval was performed by washing the slides 3× in Xylene for 5 minutes, 2× in 100% ethyl alcohol (ETOH) for 2 minutes, 2× in 95% ETOH for 2 minutes, 2× in 70% ETOH for 2 minutes, 1× in 40% ETOH for 2 minutes, and 1× in H_2O (tap) for 5 minutes. Antigen retrieval was performed in Tris-EDTA buffer (10 mmol/L Tris Base [Fisher BioReagents; Thermo Fisher Scientific], 1 mmol/L EDTA [KD Medical, Columbia, Md], 0.05% Tween 20, pH 9.0). Tris-EDTA buffer was brought to boiling and placed in rice cooker with boiling water. Slides were added to the hot Tris-EDTA buffer for 20 minutes and washed in cold tap water for 10 minutes after. For optical cutting temperature medium sections, optical cutting temperature medium was removed by washing slides in PBS at RT for 10 minutes. Slides were then blocked and stained as described above. Z-stack or snap images were taken with a Zeiss LSM 800 microscope (Carl Zeiss AG, Oberkochen, Germany). For quantification analysis, 1 field of view from each well was imaged randomly and the percentage of total HOXA3-positive cells over total DAPI-positive cells was quantified by hand using ImageJ software (National Institutes of Health, Bethesda, Md). Antibodies are as follows: anti-mouse Cd3 (100220; BioLegend, San Diego, Calif) 1:50, CD205 (MA5-34695; Thermo Fisher Scientific) 1:100, EPCAM (324202; BioLegend) 1:200, FOXA2 (07-633; Millipore, Burlington, Mass) 1:300, HOXA3 (sc-374237; Santa Cruz Biotechnology, Dallas, Tex) 1:100, KRT5 (ab52635; Abcam, Cambridge, UK) 1:100, KRT8 (sc-8020; Santa Cruz) 1:100, NANOG (ab77095; Abcam) 1:300, OCT4 (sc-5279; Santa Cruz) 1:100, panKRT (ab9377; Abcam) 1:300, SOX2 (ab97959; Abcam) 1:500. Graft staining for mouse CDs was performed by the Human Immunology and Immunotherapy Initiative at the University of Colorado Anschutz Medical Campus.

Flow cytometry (mouse cells)

Collected mouse tissues were dissociated in Dulbecco modified Eagle medium containing 1 mg/mL collagenase IV (LS004189; Worthington, Lakewood, NJ) at 37°C for 1.5 hours. Cells were filtered (40 μm) and red blood cells lysed in ACK Lysing Buffer (A1049201; Life Technologies, Thermo Fisher Scientific) before resuspension in PBS containing 2% FBS for analysis. White blood cells were separated from whole blood by ammonium-chloride-potassium lysis and centrifugation. Cells were washed and stained with the mouse antibodies CD3 and CD45 at a 1:10 concentration (100235, 103105; BioLegend). Cytometric analysis was conducted on a CyAn ADP (Beckman Coulter, Fort Collins, Colo) and analyzed using Summit V5.1 (Beckman Coulter) software.

Immunohistochemistry

Slides were deparaffinized and rehydrated in graded concentrations of alcohol before antigen retrieval in citrate buffer, pH 6 (S1699; Dako, Carpinteria, Calif) at 50°C for 10 minutes and rinsed in wash buffer (K8007; Dako). All staining was done in a Dako Autostainer. Slides were incubated in dual endogenous enzyme block (S2003; Dako) for 10 minutes, protein-free blocking solution (X0909; Dako) for 20 minutes and then in primary antibody for 60 minutes. Primary antibodies and dilutions: mouse CD45 (550539; Becton Dickinson Biosciences, San Jose, Calif), 1:400; mouse CD3 (MAB4841; R&D Systems), 1:50. Staining was developed as follows: EnVision + Dual Link System HRP; (K4061Dako) for 30 minutes and substrate-chromogen (DAB+) Solution (K3468; Dako) for 5 minutes. Slides were counterstained with hematoxylin (S3301; Dako) for 10 minutes. Quantification of cells was performed by counting staining in ≥3 nonoverlapping fields on a Zeiss Axio Imager A2 microscope.

T-cell activation assay

Splenocytes/lymph node cells from sham and TEP-grafted mice were prepared by lysing the red blood cells then purifying them through negative selection for CD4 and CD8 (130-095-130; Pan T-cell Isolation Kit II mouse; Miltenyi Biotec, Teterow, Germany). These cells were then plated and stimulated with plate-bound anti-CD3 (145-2C11, 10 μg/mL) and soluble anti-CD28 (35.11, 1 μg/mL) for 24 hours. After 24 hours cells were harvested and analyzed for their activation status by flow cytometry with antibodies against the following cell surface markers (Thy1.2 APC [553007; BD Biosciences], CD25 PE [553075; BD Biosciences], CD69 PE [553237; BD Biosciences], CD4 FITC [553729; BD Biosciences], CD8a PacBlue [100725; BioLegend]). Lymphocytes were gated on with Thy1.2 and then subgated by CD4 and CD8 to analyze cell surface expression levels of the activation markers, CD69 and CD25. Expression levels were compared to the $Thy1^-$ population as a control between the sham and TEP-grafted cells.

Cell preparation for scRNAseq

Graft was carefully dissected from resected kidney and placed in 0.25% trypsin at 4°C for 2 to 2.5 hours. Graft and trypsin mixture was then placed at 37°C for 5 minutes, vortexed and passed through 35-μm filter, counted using a hemocytometer, and diluted to a concentration of 100 to 2000 cells/μL. For primary thymus samples, a small ~1-cm^3 section of tissue was dissected, minced with a razor blade, and incubated in 0.25% trypsin for 1.5 hours at 4°C. A second ~1-cm^3 section of tissue was dissected and mashed against a 35-μm filter. The tissue section was washed 5× with PBS with mechanical agitation, in an attempt to deplete the sample of thymocytes and enrich for the epithelial cell compartment. Thymocyte-depleted section was then minced with a razor blade and placed in 0.25% trypsin for 1.5 hours at 4°C. Tissue and trypsin mixture were then placed at 37°C for 5 minutes, vortexed, and passed through 35-μm filter, counted using a hemocytometer, and diluted to a concentration of 100 to 2000 cells/μL. Cell suspensions were then taken to the University of Colorado Anschutz Medical Campus Genomics and Microarray Core for single-cell sequencing on a 10× Genomics Chromium Box (Pleasanton, Calif).

RNA preparation for bulk sequencing

For d19 TEPs, 1 well of a 24-well plate was collected and resuspended in 350-μL Qiagen RLT lysis buffer. For grafts, TEP grafts were dissected from resected kidney, and a small portion was placed in 350-μL Qiagen RLT lysis buffer. Graft was then homogenized using an electronic pellet pestle (749540-0000; Kimble). For primary thymus, a small ~1- to 2-mm^3 section of tissue was placed in 500 μL of RLT lysis buffer. RNA was isolated using QIAGEN RNeasy Mini Kit, as per manufacturer's instructions.

Statistics

Data were analyzed using GraphPad Prism software (La Jolla, Calif). Student *t*-test or 1-way ANOVA were performed on the ΔΔCt values or relative

TABLE I. qPCR probes used

Probe target	Supplier: assay ID
ACTB	Thermo Fisher: Hs01060665_g1
ACTB	Thermo Fisher: Hs99999903_m1
AIRE	Bio-Rad: qHsaCIP0029272
CCL25	Thermo Fisher: Hs00608373_m1
CCXL12	Thermo Fisher: Hs00171022_m1
DLL4	Bio-Rad: qHsaCEP0051500
EYA1	Thermo Fisher: Hs00166804_m1
FOXN1	Thermo Fisher: Hs00919266_m1
HLA-DRA	Bio-Rad: qHsaCEP0040019
HOXA3	Thermo Fisher: Hs00601076_m1
KRT5	Bio-Rad: qHsaCEP0055058
KRT8	Bio-Rad: qHsaCEP0041467
NANOG	Bio-Rad: qHsaCEP0050656
OCT4	Bio-Rad: qHsaCEP0041056
SOX2	Bio-Rad: qHsaCEP0039595

TABLE II. qPCR primers used

Target	Primer sequence
ACTB F	CATGTACGTTGCTATCCAGGC
ACTB R	CTCCTTAATGTCACGCACGAT
NANOG F	CCCCAGCCTTTACTCTTCCTA
NANOG R	CCAGGTTGAATTGTTCCAGGTC
OCT4 F	CCGAAAGAGAAAGCGAACCAG
OCT4 R	ATGTGGCTGATCTGCTGCAGT
SOX2 F	CCATGACCAGCTCGCAGAC
SOX2 R	GGACTTGACCACCGAACCC

quantification values, as indicated in figure legends. Error bars in bar graphs represent the SEM.

Single-cell sequencing

Libraries were prepared and run on Illumina and 250 million reads were captured for all the 4 samples. The reads were aligned using the 10× Genomics,[21] Cell Ranger pipeline to generate feature-barcode matrices. Both human and mouse references (GRCH38-and-mm10) were used to align the individual xenograft sample reads. The number of cells captured in the thymus samples was 8515 followed by 5500 cells in thymus-depleted, 4042 in EEE1, and 1602 cells in HM74 samples. The mean reads per cell ranged from 151,767 to 50,644 across the samples. The raw feature-barcode matrices of each sample were combined in R (R Foundation, Vienna, Austria) and analyzed using the Seurat (3.1.0) pipeline.

Preprocessing. The cells were filtered on the basis of number of unique genes in each cell and the percentage of mitochondria present. Cells with <250 genes and >5000 genes were discarded. Cells having more than 5% human and mouse mitochondrial content were not analyzed further as higher mitochondrial content correlates with low-quality or dying cells. The data was normalized using the log normalize method to a scale factor of 10,000. For feature selection, variation-stabilizing transformation was applied, as is detailed by Stuart et al,[22] to return 5000 features per dataset. Next, linear transformation (scaling) was performed prior to linear dimensionality reduction. The cells were clustered based on their principal component analysis score, first a K-nearest neighbor graph is constructed based on the Euclidean distance in principal component analysis space and then the cells are clustered by applying the Louvain algorithm. Nonlinear dimensionality reduction was done to generate the t-stochastic neighbor embedding (tSNE) plot.[23] The cells were identified, and the differentially expressed genes were found using the Wilcoxon rank sum test. To find the markers for every cluster compared with markers for the rest of the cells, Seurat function FindAllMarkers was used, the min.pct was set at 0.1 and logfc.threshold was set at 0.25, implying that the features had to be expressed by a minimum of 10% of the cells and have a log-fold change >0.25.

Pseudotime analysis

The pseudotime analysis was done using the Monocle pipeline.[24,25] The phenotype data and feature data were extracted from the Seurat object, and the Monocle CelldataSet class was created. First low-quality cells were filtered out to remove dead or empty wells in plate as well as doublets and triplets. This was done by setting minimum expression to 0.1 and num_cells_expressed ≥10. The cells were clustered without marker genes and the differentially expressed genes were found out. Monocle uses an algorithm to learn the changes in gene expression as cells go through the biological changes and places them along a trajectory. The dimensionality was reduced, and the cells were plotted along the trajectory based on the clusters as well as the original samples. The pseudotime dependent genes were found out separately for the mouse T cells and the TEPs plus TECs and plotted on a heatmap.

Velocity plot

The velocity plot was constructed using the Velocyto pipeline.[26] The pipeline was run on the Cell Ranger output using the combined reference genomes to generate a loom file that has the splicing information. The embeddings were taken from the Seurat object loaded on R and the distance between the cells were estimated. The gene relative velocity of the spliced and unspliced objects was estimated, and the velocity was shown on the Seurat tSNE embeddings.

Bulk RNAseq

RNAseq reads were generated from the Illumina sequencing platform. Sequencing quality and adapters were checked using FastQC version 0.11.5.[27] STAR (version 2.6.0c)[28] was used to compare and align the sequencing reads to the human reference genome (Homo_sapiens. GRCh38.91).[29] The reads were counted using Feature Count,[30] and values were generated for the reads per kilobase of transcript, per million mapped reads. Downstream analysis was done using R package EdgeR (version 3.14).[31] Negative binomial distributions were used to calculate biological and technical variability. Differential gene expression was determined using Fisher exact test. False discovery rate was controlled using the Benjamini-Hochberg procedure,[32] and a cutoff criterion of the false discovery rate < 0.05 was applied to identify differentially expressed genes. Differentially expressed genes were selected based on fold-change (>= |2|), and False discovery rate value ($q < 0.05$). Principal component analysis plots and Volcano plot based on -log P value versus log-fold change were created using ggplot2 in R. ComplexHeatmap version 1.10.2 package of Bioconductor was used to perform hierarchical clustering and generate Heatmap.[33]

RESULTS

Generation of TEPs from patient-derived iPSCs by direct differentiation

Based on previous differentiation protocols for the generation of TEPs *in vitro* from hESCs,[16,17] we wished to generate patient-derived TEPs from iPSCs. Throughout this study we used multiple iPSC lines, generated from distinct somatic cell sources by different reprogramming methods. The iPSC lines CB3, CB5, and CB74 were generated in-house from cord blood–derived PBMCs and C8 and C9 were generated in-house from PBMCs isolated from adult donors using nonintegrative episomal vectors as described by Okita et al[20] (see Fig E1, *A* in this article's Online Repository at www.jacionline.org; see also the Methods section). NHDF2.1 and NHDF2.2 were generated from human neonatal dermal fibroblasts utilizing RNA-based reprogramming as described previously.[34] The iPSC lines express

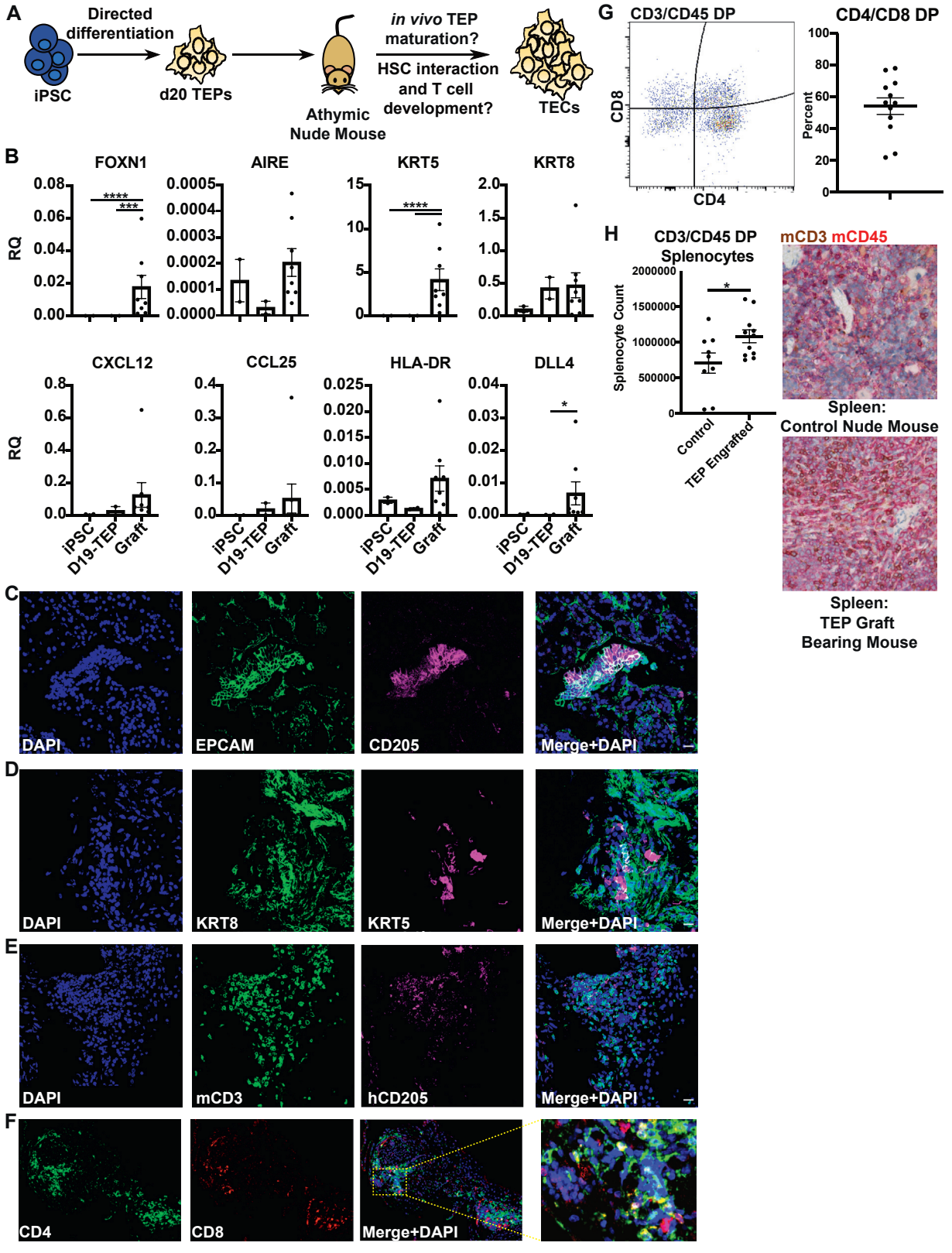

FIG 2. *In vivo* maturation of iPSC-derived TEPs to TECs. **(A)** Experimental design for *in vivo* maturation of iPSC-derived TEPs to TECs. **(B)** qPCR analysis of iPSC-derived TEPs generated using condition 4 (n = 2, 2 iPSC lines), and grafts from nude mice (n = 8). *P* values of ΔΔCt values: FOXN1: ****$P \leq .0001$, ***$P = .0001$. KRT5: $P \leq .0001$. DLL4: $P = .041$. **(C-F)** Representative IF image of TEP grafts stained for **(C)** TEC markers EPCAM (*green*) and CD205 (*magenta*); **(D)** cTEC and mTEC markers KRT8 (*green*) and KRT5 (*magenta*); **(E)** mouse T-cell marker CD3 (*green*) and human TEC marker, CD205 (*magenta*); **(F)** mouse

pluripotency marker transcripts and proteins, OCT4, SOX2, and NANOG, by quantitative PCR (qPCR) and immune fluorescence staining at levels comparable to control Mel1 hESCs (Fig E1, *B* and *D*). All, but 1 iPSC line assayed exhibit a normal karyotype (Fig E1, *C*). Cell line NHDF2.2 contains a trisomy of chromosome 14, a common abnormality in iPSCs, in all cells analyzed by g-band karyotyping, which is likely the result of previous targeting of a fluorescence reporter to the endogenous *FOXN1* loci in this cell line. Thus, after initially employing NHDF2.2 in some experiments we did not utilize this cell line further in our laboratory. Building on our previous findings,[16] we tested the effects of distinct changes to signaling pathways at the definitive endoderm and/or TPP stages on FOXN1 expression at the TEP stage using NHDF2.1 iPSCs (Fig 1, *A* and *B*). We found that all conditions tested induce robust transcript expression of TPP markers, HOXA3 and EYA1, by d9 of the differentiation protocol (Fig 1, *C*). HOXA3 and EYA1 expression increased and remained high at d14 of all differentiation protocols (Fig 1, *D*). Of all conditions tested, condition 4 induced the highest levels of FOXN1 transcripts at both d9 and d14 (Fig 1, *C* and *D*). Thus, we proceeded to evaluate condition 4 in greater detail using additional iPSC lines, CB3, CB5, and NHDF2.2 in addition to NHDF2.1. Immunofluorescence (IF) analysis and quantification of the TPP marker HOXA3 revealed about 45% of all cells are HOXA3-positive at d9 (Fig 1, *E* and *F*). qPCR analysis at d14 shows robust induction of TPP markers, HOXA3 and EYA1, and reproducible expression of TEP marker FOXN1 (Fig 1, *G*). When compared with previously published TEP-directed differentiation protocols for hESCs, our optimized condition 4 resulted in higher expression levels of *FOXN1, HOXA3,* and *EYA1* (see Fig E2, *A* in this article's Online Repository at www.jacionline.org). In the absence of a reliable human antibody for FOXN1, we used EPCAM and CD205 protein staining to quantify TEP generation. EPCAM in conjugation with other surface proteins has been widely used to identify thymic cells.[11] CD205 has been shown to mark both TEPs and cortical TECs in mice[35] and, more recently, to also identify human TEC populations.[36] Flow cytometric analysis at d14 revealed about 90% EPCAM single-positive and 45% EPCAM and CD205 double-positive cells using differentiation condition 4 (Fig 1, *H*). Using this protocol, we yield an average of 2.2×10^6 cells at d14 from 0.6×10^6 iPSCs plated 1 day before starting the differentiation protocol (Fig E2, *B*). Of note, other lineage markers that would indicate off-target differentiation are only expressed at low levels (Fig E2, *C*). In sum, we have established a directed differentiation protocol for the efficient generation of TEPs from human iPSCs derived from multiple donors employing different reprogramming technologies.

In vivo maturation of patient-derived TEPs into functional TECs

It is known that TEPs require interactions with hematopoietic stem and progenitor cells to mature into functional TECs.[8-10] Thus, to assess the ability of iPSC-derived TEPs to mature into functional TECs, we transplanted TEPs differentiated using condition 4 from 4 iPSC lines (NHDF2.2, CB74, C8, and C9) under the kidney capsule of athymic nude mice, as previously described[16] (Fig 2, *A*). Of note, in these experiments we did not add mesenchymal or any other supporting cells to the graft, as has been described previously by others,[16,17] to allow for testing of the differentiation ability of iPSC-derived TEPs without potentially confounding factors by such cell types. Mice were euthanized 14 to 19 weeks posttransplantation, and graft-bearing kidneys were prepared for multiple downstream analyses. qPCR analysis of dissected thymic grafts in comparison to *in vitro* TEPs indicates a robust induction of mature TEC markers *FOXN1*, cytokeratins *KRT5* and *KRT8*, cytokines *CXCL12* and *CCL25*, *HLA-DR (MHC-II),* and *DLL4*, suggesting further differentiation *in vivo* (Fig 2, *B*). IF staining of graft sections revealed $EPCAM^+$ epithelial structures, some of which also stained positive for the thymic marker CD205 (Fig 2, *C*). Further IF analysis showed abundant KRT8 staining, a marker for developing and cortical TECs, and to a lesser degree medullary TECs marked by KRT5 staining (Fig 2, *D*). In addition, we found KRT8 and KRT5 double-positive, developing TECs within grafts. Staining graft sections with a mouse-specific Cd3 antibody revealed an abundance of mouse T cells intermingled with human thymic cells marked by CD205 (Fig 2, *E*). Of note, we find variability in the number of cells expressing CD205 in the excised grafts (Fig 2, *C* and *E*). Further analysis using Cd4 and Cd8 IF stainings identified developing, double-positive T cells among single-positive T cells in close proximity to epithelial structures (Fig 2, *F*). To further investigate whether iPSC-derived thymus grafts can support the development of mouse T cells, spleens from engrafted and sham control mice were harvested at the time of graft removal. Flow cytometric–based quantification shows on average 50% (2043 cells ± 2577) CD4/CD8 double-positive, developing T cells within all CD3-/CD45-positive cells found in TEP grafts (Fig 2, *G*, and see Fig E3, *A* in this article's Online Repository at www.jacionline.org). Flow cytometric quantification and protein staining of peripheral CD3/CD45 double-positive T cells revealed significantly more T cells in spleens of graft-bearing mice when compared with control animals (Fig 2, *H*). Isolated splenocytes of graft-bearing mice can be readily activated by anti-Cd3/anti-Cd28 bead incubation, which is indicative of a functional T-cell phenotype (Fig E3, *B*). Of note, previous reports have shown the presence of T cells in the spleen and lymph nodes of athymic nude mice, despite the absence of a functional thymus.[37,38] In sum, these data indicate that iPSC-derived TEPs have the ability to further differentiate into patient-derived TECs *in vivo* and exhibit the ability to facilitate T-cell development in athymic nude mice.

Bulk RNAseq was performed on 2 TEP samples differentiated from 2 different iPSC lines (CB74 and NHDF2.2) and 2 corresponding grafts derived from each, for a total of 4 graft samples. Two primary neonatal thymi served as controls. Principal component analysis based on differentially expressed

T-cell markers, CD4 (*green*) and CD8 (*red*). **(C-F)** Nuclei counterstained with DAPI. Scale bar = 20 μm. **(G)** Representative flow plot and quantification of developing mouse T cells isolated from TEP grafts (n = 9 control, 12 engrafted mice, 2 cell lines). **(H)** Quantification of mouse CD3/CD45 double-positive splenocytes isolated from the spleens of nude, control mice, and nude, TEP engrafted mice. **P* = .0332. Representative immunohistochemistry image of control and TEP engrafted nude mouse spleens stained for mouse CD3 (*brown*) and CD45 (*red*). *HSC*, Hematopoietic stem and progenitor cell.

genes shows that samples are located within 3 distinct clusters reflecting their respective origin, with 1 of the TEP graft samples located in between the clusters (Fig 3, *A*). Similarly, dendrogram hierarchical clustering of whole genome expression data of all samples shows clustering of TEP samples, primary thymi and grafts, with 1 graft sample clustering closer than the other 3 graft samples to the starting TEP population (Fig 3, *B*). Next, we performed differential gene expression analysis between the sample groups. Comparing grafts versus TEPs shows 1299 and 1245 significantly upregulated and downregulated genes, respectively. Examining specific genes, TPP markers HOXA3 and EYA1 are significantly downregulated in the grafts (Fig 3, *C*), while mature TEC markers FOXN1, KRT5, and TP63 are significantly upregulated, indicating further differentiation of transplanted TEPs into patient-derived TEC grafts (Fig 3, *C*). mRNA transcript levels of the cTEC marker KRT8, compared with TEPs, were downregulated in grafts. KRT8 is primarily expressed in cTECs, however, previous studies have shown that TEPs exhibit a cTEC-like phenotype.[11,35] In line with this observation, KRT8 is also significantly less expressed than are TEPs in primary thymi, indicating that this result likely reflects normal expression changes on human TEP to TEC differentiation (Fig 3, *D*). Probing global differential gene expression of primary human neonatal thymi versus TEPs revealed 932 and 656 genes were significantly upregulated and downregulated, respectively (Fig 3, *D*). As expected, specific TEC markers, FOXN1, KRT5, TP63, CBX4, and AIRE, are significantly upregulated in primary thymi. TEP markers HOXA3 and EYA1, as well as KRT8, are expressed at lower levels than are d19 TEPs in primary thymi. Direct comparison of expression levels of thymi to grafts shows 2435 and 1737 genes were significantly upregulated and downregulated, respectively (Fig 3, *E*). However, key TEC markers, FOXN1, KRT5, KRT8, TP63, and CBX4, are present at similar levels in both groups (Fig 3, *E*). Expression levels of AIRE, a critical regulator of negative T-cell selection in the medulla, are lower in grafts. This result might reflect mismatch interactions of the receptor activator of NF-κB and its ligand by developing mouse T cells and differentiating human thymic tissue employing the xenogenic nude mouse model system that prevents thymic maturation into AIRE-positive mTECs. In sum, these data indicate that iPSC-derived TEPs are able to develop into functional, patient-derived TECs when transplanted *in vivo*.

scRNAseq resolves thymic cell types in iPSC-derived grafts and human primary neonatal thymus

In conjunction with bulk RNAseq, grafts and human primary neonatal thymus were subjected to scRNAseq analysis using 10× Genomics technology. The primary human neonatal thymus samples, referred to as Thy7.1 and Thy7.2, were derived from the same individual; however, single-cell suspensions were prepared by 2 different methods to reduce digestion time that could potentially confound gene expression levels while simultaneously enriching for the TEC fraction in Thy7.2 (see Methods section). While this approach did slightly increase the percentage of TECs detected by scRNAseq from 2.50% in Thy7.1 to 4.58% in Thy7.2, T cells still made up 79.24% of Thy7.2 single-cell fraction, a small reduction from 87.27% in Thy7.1 (data not shown). To resolve different cell types in TEP graft and human primary neonatal thymus samples, unsupervised machine learning, including tSNE,[39] was employed. This methodology effectively separates individual cells by tissue type and species (Fig 4, *A* and *B*), with 13 distinct clusters identified based on a Louvain algorithm variant[40] (data not shown). Using a comprehensive annotated list of marker genes, we further combined the 13 original clusters into 6 cell-type–specific clusters consisting of human T cells, dendritic cells, TECs, TEPs, mouse T cells, and other host cells (Fig 4, *A* and *D-G*; see Fig E4, *A-E* in this article's Online Repository at www.jacionline.org). Surprisingly, we observe the classification of some human T cells within the TEP graft single cell datasets. Individual human and mouse cells could be successfully identified using the Cell Ranger pipeline for human and mouse datasets, verifying the 6 cell-type–specific clusters based on their species (Fig 4, *B*). As expected, tSNE analysis by species shows mouse-derived cells are present only in the TEP graft samples, with no mouse cells identified in the human primary neonatal thymus samples (Fig 4, *B-C* and Fig E4, *F*). Notably, TEP graft-derived cells cluster with primary thymi cells in the TEP/TEC clusters, indicating that transplantation of iPSC-derived TEPs *in vivo* results in the generation of patient-derived TECs that transcriptionally closely resemble *bona fide* primary TECs (Fig 4, *A* and *C* and Fig E4, *F*). Next, we used violin plots to visualize the expression patterns of individual genes in our single-cell datasets and verify the validity of cell-type–specific clustering. Thymic-specific markers *FOXN1, EPCAM, KRT5,* and *KRT8* are most highly expressed in the TEP and TEC clusters, as compared to all other cell types (Fig 4, *E* and Fig E4, *C*). Key cTEC markers, *PRSS16* and *PSMB11*, are also specifically expressed in the TEC cluster (Fig 4, *E*). *CD205* is known to be present in TEPs and TECs,[11,35] and is expressed, albeit at low levels, in the TEP and TEC clusters (Fig 4, *G* and Fig E4, *E*). Additionally, key cytokines, *CXCL12* and *CCL25*, known to be expressed by thymic cells to attract hematopoietic stem cells,[41] are expressed by cells of the TEC cluster (Fig 4, *E* and Fig E4, *C*). Activin A has recently been implicated in the induction of TEP differentiation toward TECs.[42] Indeed, *INHBA*, a subunit of activin A, is expressed specifically in the TEP cluster (Fig 4, *E* and Fig E4, *C*), indicating that activin A may also play a role in human TEC development. While NOTCH signaling is critical for T-cell commitment and development,[43] we find *DLK1* is highly expressed only in the TEP population (Fig 4, *E* and Fig E4, *C*), suggesting a potential role for this pathway in human TEC differentiation. Utilizing our *in vitro* protocol to generate TEPs from iPSCs, we performed direct differentiation experiments in the presence of gamma secretase inhibitor (XXi) to inhibit NOTCH signaling during the last 7 days of the protocol. We observed a statistically significant reduction in the expression of thymic markers *FOXN1* and *KRT8*, while *KRT5* expression was very low and had not changed from control conditions (Fig 4, *H*). These results suggest a role for NOTCH signaling in human thymus development, which is in line with recent reports showing a role for NOTCH signaling in murine thymic development and TEC subtype specification.[44,45] Within the T-cell compartment, key markers of developing T cells are detected, such as progenitor and developing T-cell markers CD5 and CD7; RAG1 and RAG2; and CD3, CD4, and CD8 (Fig 4, *F* and Fig E4, *D*). Lastly, dendritic cell markers, some of which are known to be expressed by TECs also, are strongly expressed in the T-cell, dendritic-cell, and TEC compartments (Fig 4, *G* and Fig E4, *E*). Our analysis provides novel insights into expression patterns and their changes

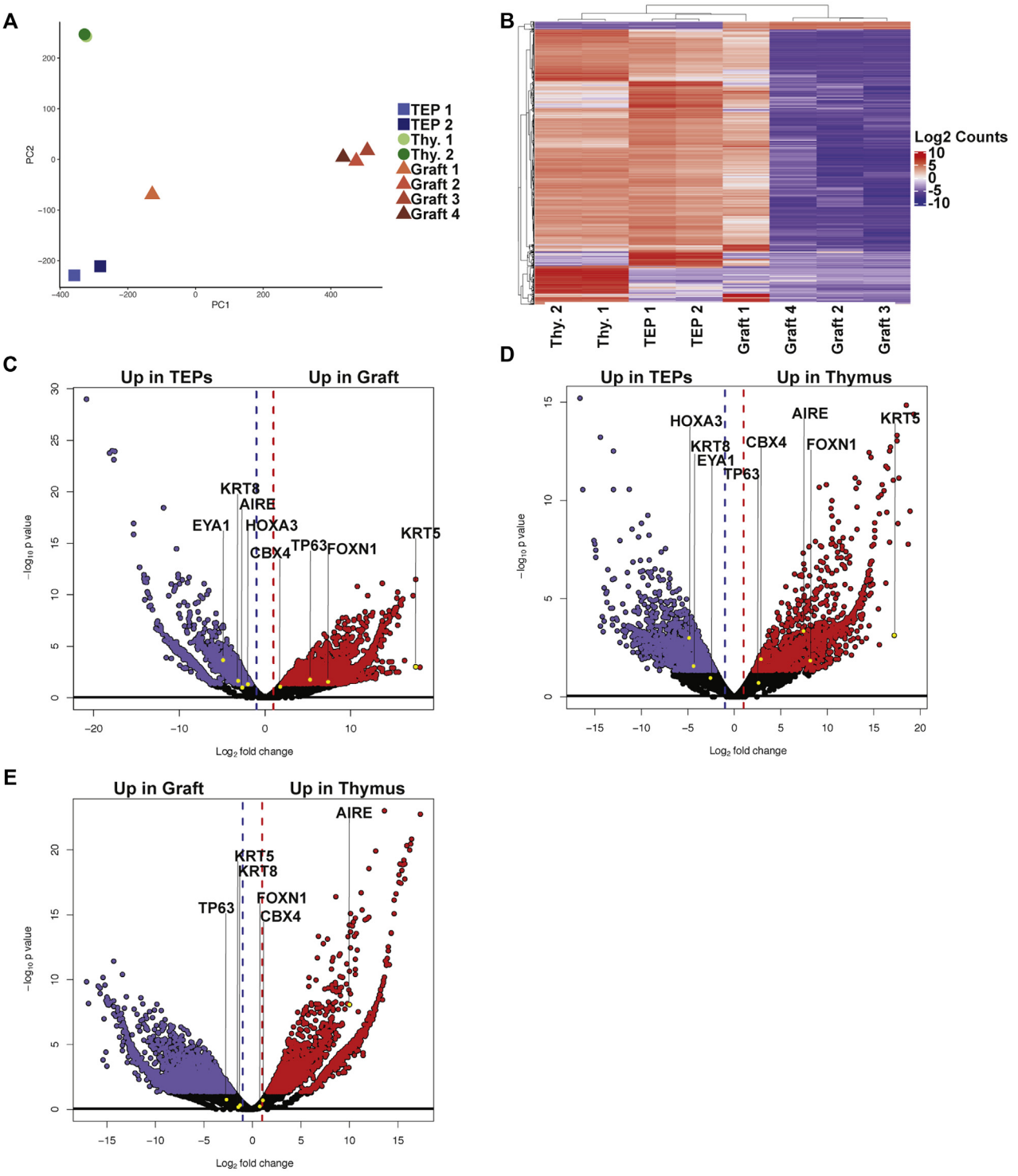

FIG 3. *In vivo* generated TECs express mature TEC markers. **(A)** Principle component (*PC*) analysis of bulk RNAseq samples showing clustering of d19 TEPs, *in vivo* generated TEC grafts, and primary neonatal human thymus (TEPs, n = 2; grafts, n = 4; primary thymus, n = 2). **(B)** Dendrogram showing whole genome hierarchical clustering of bulk RNAseq samples. **(C-E)** Significance analysis of differential gene expression displayed as volcano plots of primary neonatal thymus, TEC grafts, and d19 TEPs with TPP and key thymus markers annotated. Significant *P* values are <.01, minimum fold change 0.5 log. **(C)** Graft versus d19 TEPs. **(D)** Primary neonatal thymi versus d19 TEPs. **(E)** Primary neonatal thymus versus graft.

in distinct human thymic cell types, both stem cell–derived and neonatal. We further show that these data can be exploited to successfully identify novel signaling pathways during human thymus development. All scRNAseq data have been hosted on the Russ lab server (http://www.russlab.com/scRNA/) using UCSC Cell Browser (https://cellbrowser.readthedocs.io/).

iPSC-derived TECs cluster with primary neonatal human thymus TECs

To further resolve the cell types within the TEP/TEC clusters, we subset and reanalyzed the TEP and TEC clusters together (Fig 5, *A* and *B*). tSNE analysis identified 9 clusters within the combined TEP and TEC cell population (Fig 5, *B*, and see Fig E5, *B* in this article's Online Repository at www.jacionline.org). Sample-specific tSNE analysis shows the distribution of TEP/TEC cells throughout the newly generated clusters (Fig 5, *C*). Importantly, iPSC-derived TECs cluster together with primary thymus TECs in clusters 0 and 4, while clusters 1, 3, 7, and 8 are composed almost exclusively of iPSC-derived TEPs or TECs, suggesting that these clusters may contain developing thymic cells not readily present in the postnatal primary thymus sample (Fig 5, *B* and *C*). Indeed, utilizing markers identified from previously published single-cell sequencing experiments of developing primary thymi, the data indicate that cluster 0 contains cells with a neuroTEC signature expressing *NEUROD1* and *CHGA* (Fig 5, *G* and Fig E5, *A*).[46] Clusters 1 and 3 present as TEP/intermediate "mcTEC" cells, as indicated by the presence of *HOXA3* transcripts in cluster 1, and *DLK1, KRT8, KRT14,* and *INHBA* in cluster 3, respectively (Fig 5, *G* and Fig E5, *A*).[46] Coexpression of key markers *FOXN1, KRT5, KRT8*, and *DLK1* in a large number of cells in cluster 3 indicates that the majority of all TEPs are contained in this subset (Fig 5, *G* and Fig E5, *A*). TEC markers *PSMB11, PRSS16,* and *CCL25*, as well as individual expression of *KRT5* or *KRT8,* are present in cells of cluster 5 at moderate to high levels, indicating a more mature TEC population (Fig 5, *G* and Fig E5, *A*). *KRT5* is expressed by more cells and at slightly higher levels in cluster 5 than in cluster 7; however, a very low number of cells in cluster 5 also express *AIRE* (Fig 5, *G* and Fig E5, *A*). As mTECs are marked by the expression of both *KRT5* and *AIRE*,[11] the data suggest that cluster 5 may represent mTECs. By distinguishing between unspliced and spliced mRNAs in scRNAseq data, RNA velocity can be used to predict the likely future state of any individual cell within the dataset.[26] RNA velocity analysis predicts the directionality of TEP graft-derived cells as moving from clusters 1 and 8 toward clusters 3 and 7 (Fig 5, *B* and *D*). Monocle's pseudotime analysis was applied to the reclustered TEP/TEC clusters, and 1 branch point was identified (Fig 5, *E* and *F*). Our detailed analysis shows that some iPSC-derived TECs and primary TECs exhibit overlapping expression profiles by the bioinformatic approaches employed. However, iPSC-derived TEPs still differentiating into TECs appear to follow 2 differential developmental trajectories, of which only 1 leads toward a primary TEC-like phenotype. This could be a result of the xenograft interaction of iPSC-derived TEPs with developing mouse T cells and warrants further investigation to implement further differentiation improvements in the future.

Mouse T cells develop within iPSC-derived thymic tissue

To determine whether *de novo* T-cell development was indeed occurring in iPSC-derived thymic grafts as suggested by our previous analyses (Fig 2, *E-H* and Fig E3), we subset and reanalyzed the mouse T-cell cluster individually (Fig 6, *A* and *B*). tSNE analysis identified 10 clusters within the mouse T-cell cluster population (Fig 6, *B*, and see Fig E6, *C* in this article's Online Repository at www.jacionline.org). Indeed, we identified surface markers and key transcription factors involved in prethymic and intrathymic mouse T-cell development are present at varying levels in many of the mouse T-cell subclusters, indicating the developmental progression of mouse T cells in nude mice that received a TEP graft (Fig 6, *F* and Fig E6, *B*).[47] Additionally, expression of Deoxynucleotidyl transferase terminal-interacting proteins 1 and 2, indicative of TCR rearrangement, is detected in many T-cell subpopulations (Fig 6, *F* and Fig E6, *B*). Pseudotime analysis shows only 1 branch point, with cells developing toward 2 cell fates (Fig 6, *C*). Gene-specific pseudotime analysis shows 3 developmental states (Fig 6, *D*). Key T-cell markers, Cd3e, Cd3g, Cd4, Cd8a, and Ptprc (Cd45), show low expression during states 1 and 2, but increased expression during state 3, indicative of the developmental progression of the mouse-derived T cells in the TEP graft (Fig 6, *D*). Additionally, we observe a small transient increase in the expression of proliferation marker Mki67 during stage 1, which is indicative of cell proliferation that is associated with T-cell development (Fig 6, *D*). During the course of development, cells branch out in different trajectories based on their developmental lineage. The branch points heatmap, made using Monocle, shows genes that are enriched at the branch point, as well as in each cell fate. In cell fate 2, we observe the enrichment of innate immune cell markers (Fig 6, *E*). Further, cell fate 1 shows enrichment for some markers of T-cell development, such as Aif1 and Tyrobp (Fig 6, *E*). Interestingly, cluster 4 cell fate 2 shows enrichment for B-cell markers, as B cells have also been shown to be present in the thymus[48] (Fig 6, *E*). Taken together, we demonstrate the presence of murine-derived cells that express markers indicative of ongoing T-cell development.

DISCUSSION

In this work we present a direct differentiation protocol to generate TEPs from all iPSC lines tested. Notably, iPSCs were generated from different somatic cell sources and by diverse reprogramming modalities. Importantly, TEPs derived from multiple iPSC lines can give rise to TECs after transplantation into athymic nude mice. TECs have the ability to educate developing mouse T cells, indicating a functional thymic cell phenotype. Indeed, scRNAseq analysis shows that iPSC-derived TECs exhibit gene expression profiles related to primary, neonatal human TECs, further corroborating the notion that our direct differentiation protocol generates relevant thymic cells. Using insights from scRNAseq analyses and direct pathway manipulation *in vitro*, we find a potentially unappreciated role for NOTCH signaling in human TEC development. In addition, these datasets provide a novel list of target genes that are likely important in human thymus development and should be further investigated. We anticipate that these findings will have a critical impact for basic

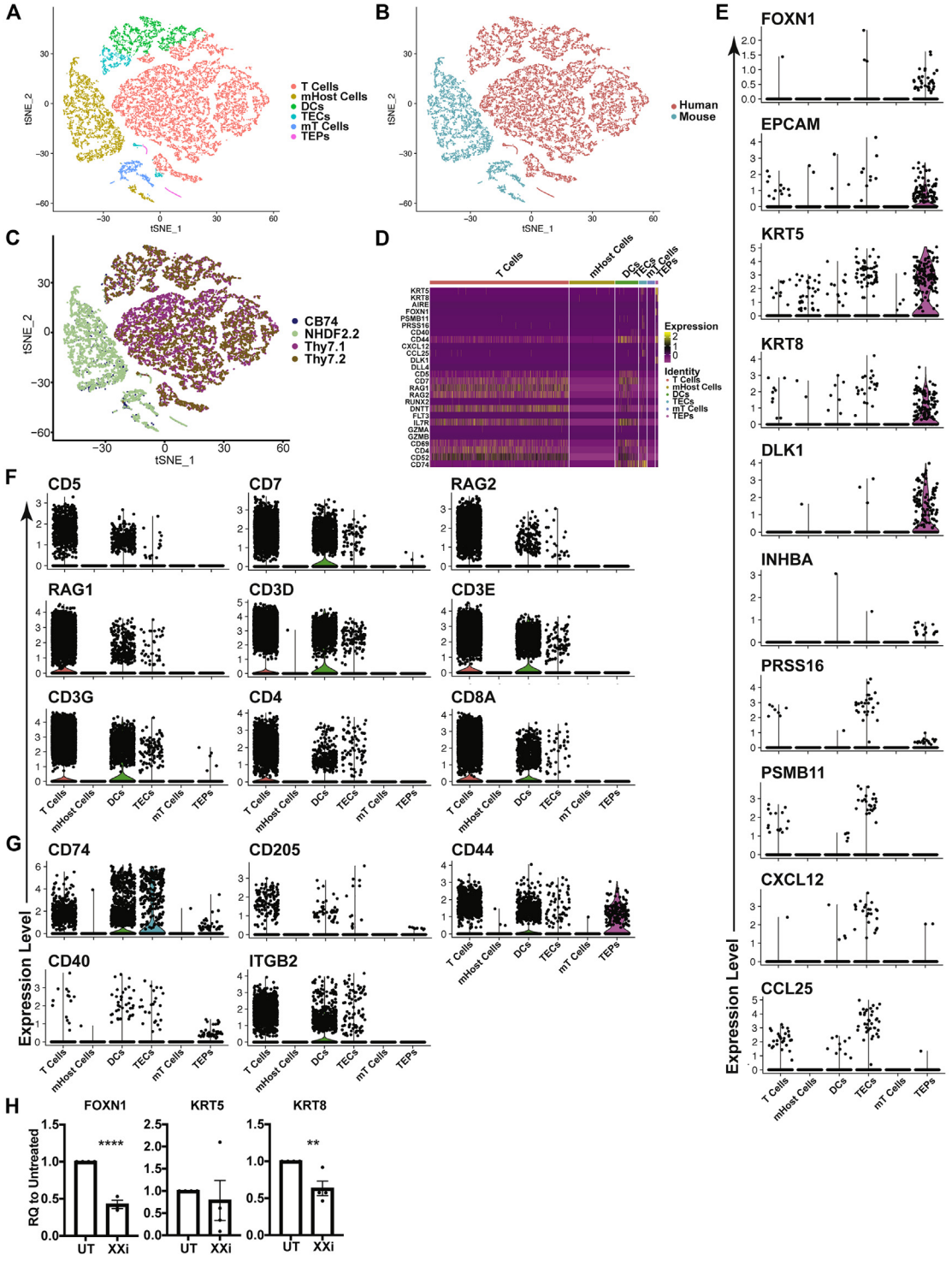

FIG 4. TEC grafts exhibit distinct cell subpopulations expected to be present in developing human thymi. **(A-C)** tSNE visualization of scRNAseq data of TEP grafts and primary human neonatal thymus samples. (Grafts, n = 2 [17 weeks]; primary thymus, n = 1 prepared by 2 different methods.) **(A)** Cluster analysis revealed distinct cell populations within samples. **(B)** Species-wise visualization of clusters corresponds to cluster labeling in Fig. 4, *A*. **(C)** Sample-wise visualization of the scRNAseq data. **(D)** Curated heatmap of common immune-related genes. **(E)** Violin plots of cluster-specific gene expression of key thymic markers. **(F)** Violin plots showing cluster-specific gene expression of human T-cell markers. **(G)** Violin plots showing cluster-specific gene expression of key dendritic and antigen-presenting cell markers. **(H)** Gene expression analysis of TEP markers FOXN1, KRT5, and KRT8 at d20 with or without treatment with NOTCH inhibition [gamma-secretase inhibitor (XXi)] starting d14. Data normalized to ACTB and set relative to untreated control (n = 4, 2 iPSC lines). *P* values of RQ values; FOXN1: ****$P \leq .0001$, KRT8: **$P = .0098$. *DC*, Dendritic cell; *mHost*, mouse host cell; *mT*, mouse T cell.

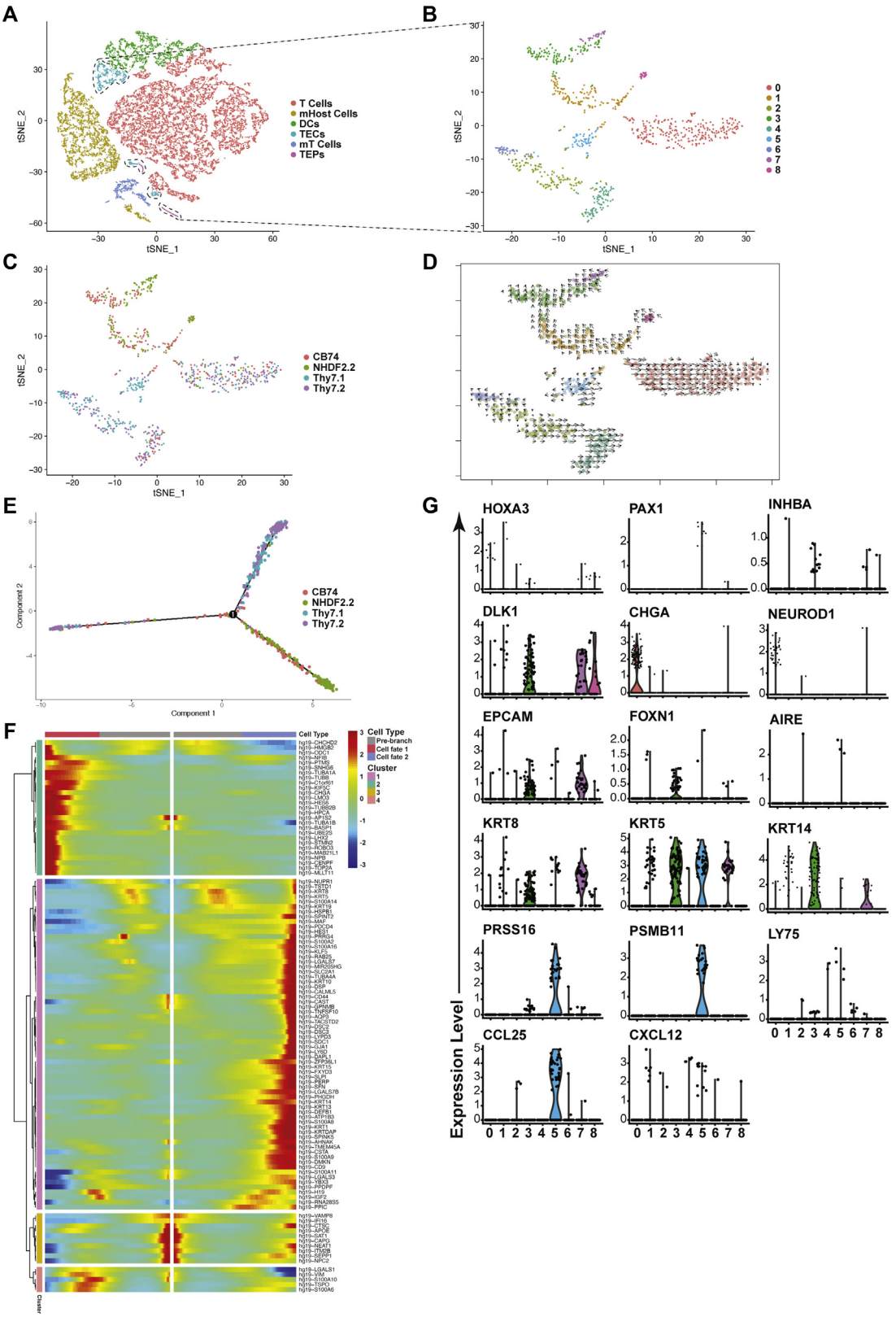

FIG 5. iPSC-derived TECs closely resemble TECs present in primary, neonatal thymus. **(A)** tSNE visualization of original cluster subpopulations with TEP and TEC clusters demarcated. **(B)** tSNE visualization following subcluster analysis of TEP/TEC populations. **(C)** Sample-wise tSNE visualization of subclustered TEC populations. **(D)** Velocity analysis showing projected developmental directionality of TEC populations. **(E)** Pseudotime analysis of TEP subpopulations showing sample-specific developmental trajectory. **(F)** Branching point heatmap showing genes differentially expressed at the branching point of the pseudotime analysis. **(G)** Violin plots of key thymic markers within the TEP/TEC populations.

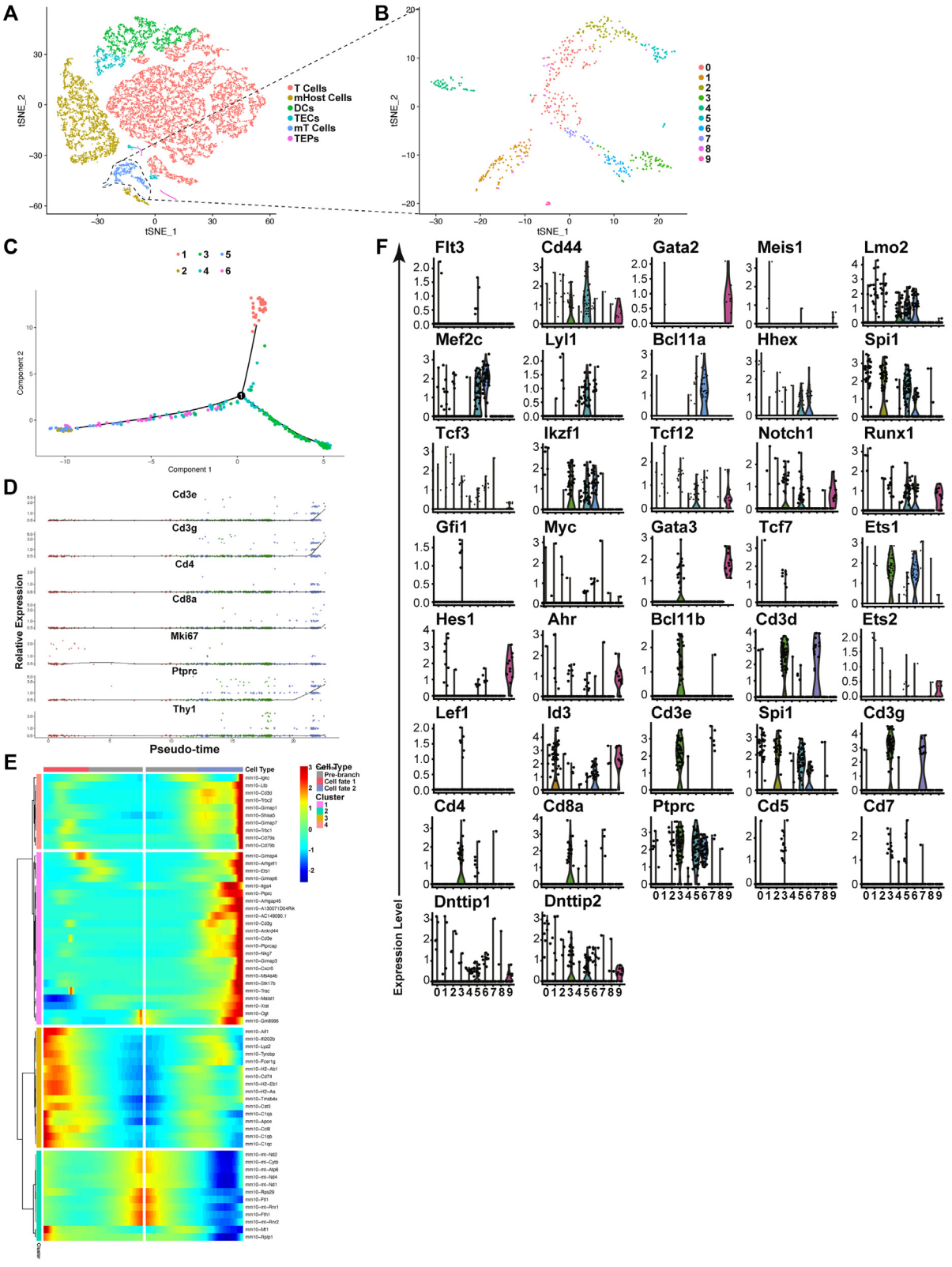

FIG 6. Subclustering of mouse-derived T cells in iPSC-derived *in vivo* matured TEP graft.**(A)** tSNE visualization of original clusters with mouse T cells demarcated. **(B)** tSNE analysis showing subclustering of mouse-derived T cells. **(C)** Pseudotime analysis of the mouse-derived T cells. **(D)** Gene-specific pseudotime trajectory of key markers of developing T cells. **(E)** Branching point heatmap showing genes differentially expressed at the branching point of the pseudotime analysis. **(F)** Violin plots of key transcription factors and cell surface markers of developing mouse T cells.

and translational research by providing a framework for researchers to generate thymic cells in a patient-specific manner.

A critical roadblock for accelerating research efforts into human thymus function and T-cell development has been the lack of an effective differentiation protocol for multiple human pluripotent stem cell lines.[18] This is illustrated by our difficulty to generate thymic cells with the majority of iPSC lines tested employing differentiation conditions reminiscent of published hESC protocols and without transgene expression. To overcome this problem, we tested the effects of specific manipulations to the retinoic, TGF-β and Hedgehog pathways during direct differentiation into TEPs using multiple iPSC lines. This approach was informed by insights from previous work evaluating the effects of individual pathways on thymus development using animal models[2,49,50] and their application to the generation of TEPs using individual human pluripotent stem cell lines described earlier.[16,17] Surprisingly, we found that after establishing an anteriorized definitive endoderm cell population at d5, despite different manipulations, all cultures efficiently gave rise to TPP cells (Fig 1, *D*). However, differences were observed at the subsequent thymic differentiation stage in the expression levels of *FOXN1* transcripts, suggesting potential effects on TEP-cell specification. To overcome difficulties in quantifying thymic cells in differentiating cultures due to the absences of a reliable antibody to detect FOXN1 protein, we employed the surface markers EPCAM and CD205. Thymic cells positive for CD205 have been shown to label both TEPs and TECs in mouse[35] and, recently, in human neonatal thymi.[36] We demonstrate here the successful utility of these surface markers for assessing the efficiency of iPSC-derived TEP generation. While additional experiments are required to develop a more comprehensive understanding of human CD205-labeled thymic cells, this surface marker likely provides an important tool for subsequent studies generating stem cell–derived thymic cells.

It is known that human fetal thymus grafts are capable of supporting murine T-cell development and partial immune cell reconstitution in congenitally athymic mice.[51] These efforts have led to many advances in the generation of humanized mouse models that recapitulate critical aspects of the human immune system. However, these models rely on the procurement and use of limited human fetal tissue, thus inhibiting the ability to interrogate various aspects of human immune function in a patient-specific manner. For TEPs to further mature into TECs, interactions with developing T cells are required.[8-10] Indeed, hESC-derived TEPs are capable of supporting T-cell development in athymic mice.[16,17] Interestingly, hESC-derived TEP grafts tend to support murine T-cell development better than human fetal thymus grafts do.[16] However, hESC-derived TEPs do not allow the generation of patient-derived model systems, potentially restricting its future use for clinically relevant investigations. Thus, we transplanted TEPs differentiated from 4 independent iPSC lines under the kidney capsule of athymic nude mice and evaluated potential differentiation into TECs by different parameters. Nude mice are athymic, due to the absence of functional Foxn1 protein, but contain hematopoietic stem and progenitor cells that can give rise to T cells if a functional thymus, either human or mouse, is provided via transplant.[52] Our analyses suggest further differentiation of iPSC-derived TEPs into functional TECs. We detect an abundance of cells stained for thymic epithelial marker proteins EPCAM, CD205, KRT8, and KRT5. Some of the epithelial structures within grafts resemble typical thymic morphology with developing mouse T cells intermingled. However, we do note that some epithelial cell structures within grafts do lack a typical thymic morphology. Recent findings suggest a critical role for thymic mesenchyme in supporting the proper organization of human thymic grafts.[36] However, we did not include mesenchymal cells in our experiments at the time of transplant. Future work should evaluate the exact function of supporting cell types on human TEP differentiation and TEC graft function.

To attain a better understanding of the gene expression changes during human thymic development, identify potential regulators, and probe for cell heterogeneity we employed both bulk RNAseq and scRNAseq analysis of *in vitro* generated TEPs, grafts containing TECs, and primary neonatal human thymi. Recent work employing scRNAseq has shown that TECs within mouse and human thymi can be further subdivided into defined cell clusters based on gene expression profiles.[46,53-55] We used bioinformatics to distinguish between mouse and human cells with high confidence and used marker expression profiles to assign specific cell functions to cluster subpopulations. The critical finding of this analysis is that a small but appreciable TEC subpopulation is present in iPSC-derived grafts and that these cells cluster together with primary TECs. Using the datasets generated, we verify that TECs, both iPSC-derived and primary, express characteristic marker genes and can be further divided into subclasses. These analyses suggest involvement of the activin A signaling pathway in TEP to TEC differentiation. This is in line with recent findings that a switch from BMP4 to activin A signaling is critical in mouse thymus development.[42] We are currently testing whether a similar switch in signaling activity can be exploited to generate human TECs *in vitro*. As *DLK1* was found to be specifically expressed within the TEP subpopulation, we hypothesized that NOTCH signaling may play role in human TEP development and found significant reduction in the thymic markers FOXN1 and KRT8 following NOTCH inhibition. Of note, 2 groups have recently shown a role for NOTCH signaling in murine TEC development.[44,45] These datasets provide important novel information on potential regulators of human thymus development and show the generation of functional patient-derived TECs using our differentiation approach.

Taken together, we provide here important resources, both a direct differentiation protocol and detailed datasets of iPSC-derived thymic cells to the research community. We anticipate that our findings will allow researchers to accelerate ongoing efforts investigating human T-cell and thymus biology.

We thank Drs Bilousova and Korbut for sharing the NDHF2.1 iPSC line and the Human Immune Monitoring Shared Resource within the University of Colorado Human Immunology for assistance with mouse T-cell analysis.

Clinical Implications: The efficient generation of thymic cells that can educate developing T cells has therapeutic implications for patients with primary thymic disorders, and it will also further preclinical identification of immune-based therapies.

REFERENCES

1. Anderson G, Lane PJL, Jenkinson EJ. Generating intrathymic microenvironments to establish T-cell tolerance. Nat Rev Immunol 2007;7:954-63.
2. Manley NR. Thymus organogenesis and molecular mechanisms of thymic epithelial cell differentiation. Semin Immunol 2000;12:421-8.
3. Nehls M, Pfeifer D, Schorpp M, Hedrich H, Boehm T. New member of the winged-helix protein family disrupted in mouse and rat nude mutations. Nature 1994;372:103-7.

4. Pignata C, Fiore M, Guzzetta V, Castaldo A, Sebastio G, Porta F, et al. Congenital alopecia and nail dystrophy associated with severe functional T-cell immunodeficiency in two sibs. Am J Med Genet 1996;65:167-70.
5. Vaidya HJ, Briones Leon A, Blackburn CC. FOXN1 in thymus organogenesis and development. Eur J Immunol 2016;46:1826-37.
6. Cheng L, Guo J, Sun L, Fu J, Barnes PF, Metzger D, et al. Postnatal tissue-specific disruption of transcription factor FoxN1 triggers acute thymic atrophy. J Biol Chem 2009Available at:https://www.ncbi.nlm.nih.gov/pmc/articles/PMC2820809/pdf/zbc5836.pdf . Accessed August 7, 2017.
7. Blackburn CC, Augustine CL, Li R, Harvey RP, Malint MA, Boydt RL, et al. The nu gene acts cell-autonomously and is required for differentiation of thymic epithelial progenitors (nude mice/thymus). Immunology 1996Available at: http://www.pnas.org/content/pnas/93/12/5742.full.pdf. Accessed November 5, 2018.
8. Shores EW, Van Ewijk W, Singer A. Maturation of medullary thymic epithelium requires thymocytes expressing fully assembled CD3-TCR complexes. Int Immunol 1994;6:1393-402.
9. Holländer GA, Wang B, Nichogiannopoulou A, Platenburg PP, Ewijk W van, Burakoff SJ, et al. Developmental control point in induction of thymic cortex regulated by a subpopulation of prothymocytes. Nature 1995;373:350-3.
10. Klug DB, Carter C, Gimenez-Conti IB, Richie ER. cutting edge: thymocyte-independent and thymocyte-dependent phases of epithelial patterning in the fetal thymus. J Immunol 2002;169:2842-5.
11. Perniola R. Twenty years of AIRE. Front Immunol 2018;9:98.
12. Harrington LE. T-cell development. In: Rich RR, editorClinical Immunology: Principles and Practice. 5th ed. New York: Elsevier Ltd; 2019. pp. 119-25.
13. Anderson MS, Venanzi ES, Klein L, Chen Z, Berzins SP, Turley SJ, et al. Projection of an immunological self shadow within the thymus by the Aire Protein. Proc Natl Acad Sci U S A 2002;298:1395-401.
14. Palmer DB. The effect of age on thymic function. Front Immunol 2013;4:316.
15. Mackall CL, Gress RE. Thymic aging and T-cell regeneration. Immunol Rev 1997;160:91-102.
16. Parent AV, Russ HA, Khan IS, Laflam TN, Metzger TC, Anderson MS, et al. Generation of functional thymic epithelium from human embryonic stem cells that supports host T cell development. Cell Stem Cell 2013;13:219-29.
17. Sun X, Xu J, Lu H, Liu W, Miao Z, Sui X, et al. Directed differentiation of human embryonic stem cells into thymic epithelial progenitor-like cells reconstitutes the thymic microenvironment in vivo. Cell Stem Cell 2013;13:230-6.
18. Chhatta AR, Cordes M, Hanegraaf MAJ, Vloemans S, Cupedo T, Cornelissen JJ, et al. De novo generation of a functional human thymus from induced pluripotent stem cells. J Allergy Clin Immunol 2019;144:1416-9.e7.
19. Yamazaki Y, Urrutia R, Franco LM, Giliani S, Zhang K, Alazami AM, et al. PAX1 is essential for development and function of the human thymus. Sci Immunol 2020;5:eaax1036.
20. Okita K, Yamakawa T, Matsumura Y, Sato Y, Amano N, Watanabe A, et al. An efficient nonviral method to generate integration-free human-induced pluripotent stem cells from cord blood and peripheral blood cells. Stem Cells 2013;31:458-66.
21. 10× Genomics. What is Cell Ranger? Official support. Available at: https://support.10xgenomics.com/single-cell-gene-expression/software/pipelines/latest/what-is-cell-ranger. Accessed April 3, 2020.
22. Stuart T, Butler A, Hoffman P, Hafemeister C, Papalexi E, Mauck WM III, et al. Comprehensive integration of single-cell data. Cell 2019;177:1888-902.
23. Butler A, Hoffman P, Smibert P, Papalexi E, Satija R. Integrating single-cell transcriptomic data across different conditions, technologies, and species. Nat Biotechnol 2018;36:411-20.
24. Trapnell C, Cacchiarelli D, Grimsby J, Pokharel P, Li S, Morse M, et al. The dynamics and regulators of cell fate decisions are revealed by pseudotemporal ordering of single cells. Nat Biotechnol 2014;32:381-6.
25. Qui X, Mao Q, Tang Y, Wang L, Chawla R, Pliner HA, et al. Reversed graph embedding resolves complex single-cell trajectories. Nat Methods 2017;14:979-82.
26. La Manno G, Soldatov R, Zeisel A, Braun E, Hochgerner H, Petukhov V, et al. RNA velocity of single cells. Nature 2018;560:494-8.
27. Chen S, Huang T, Zhou Y, Han Y, Xu M, Gu J. AfterQC: automatic filtering, trimming, error removing and quality control for fastq data. BMC Bioinformatics 2017Available at: http://creativecommons.org/publicdomain/zero/1.0/. Accessed April 3, 2020.
28. Dobin A, Davis CA, Schlesinger F, Drenkow J, Zaleski C, Jha S, et al. STAR: ultrafast universal RNA-seq aligner. Bioinformatics 2013;29:15-21.
29. Kersey PJ, Staines DM, Lawson D, Kulesha E, Derwent P, Humphrey JC, et al. Ensembl Genomes: an integrative resource for genome-scale data from non-vertebrate species. Nucleic Acids Res 2012;40:D91-7.
30. Liao Y, Smyth GK, Shi W. featureCounts: an efficient general purpose program for assigning sequence reads to genomic features. Bioinformatics 2014;30:923-30.
31. Robinson MD, Mccarthy DJ, Smyth GK. edgeR: a Bioconductor package for differential expression analysis of digital gene expression data. Bioinformatics 2010;26:139-40.
32. Benjamini Y, Hochberg Y. Controlling the false discovery rate: a practical and powerful approach to multiple testing. J R Stat Soc 1995;57:289-300.
33. Gu Z, Eils R, Schlesner M. Complex heatmaps reveal patterns and correlations in multidimensional genomic data. Bioinformatics 2016;32:2847-9.
34. Kogut I, McCarthy SM, Pavlova M, Astling DP, Chen X, Jakimenko A, et al. High-efficiency RNA-based reprogramming of human primary fibroblasts. Nat Commun 2018;9:745.
35. Baik S, Jenkinson EJ, Lane PJL, Anderson G, Jenkinson WE. Generation of both cortical and Aire + medullary thymic epithelial compartments from CD205 + progenitors. Eur J Immunol 2013;43:589-94.
36. Campinoti S, Gjinovci A, Ragazzini R, Zanieri L, Ariza-McNaughton L, Catucci M, et al. Reconstitution of a functional human thymus by postnatal stromal progenitor cells and natural whole-organ scaffolds. Nat Commun 2020;11:6372.
37. Kennedy JD, Pierce CW, Lake JP. Extrathymic T cell maturation: phenotypic analysis of T cell subsets in nude mice as a function of age. J Immunol 1992;148:1620-9.
38. Ikehara S, Pahwa RN, Fernandes G, Hansen CT, Good RA. Functional T cells in athymic nude mice. Proc Natl Acad Sci U S A 1984;81:886-8.
39. Maaten L Van Der, Hinton G. Visualizing data using t-SNE. J Machine Learn Res 2008Available at: http://www.jmlr.org/papers/volume9/vandermaaten08a/vandermaaten08a.pdf. Accessed August 22, 2019.
40. Waltman L, van Eck NJ. A smart local moving algorithm for large-scale modularity-based community detection. Eur Phys J B 2013;86:471.
41. Calderón L, Boehm T. Synergistic, context-dependent, and hierarchical functions of epithelial components in thymic microenvironments. Cell 2012;149:159-72.
42. Lepletier A, Hun ML, Hammett MV, Wong K, Naeem H, Hedger M, et al. Interplay between follistatin, activin A, and BMP4 signaling regulates postnatal thymic epithelial progenitor cell differentiation during aging. Cell Rep 2019;27:3887-901.e4.
43. Radtke F, Fasnacht N, Macdonald HR. Notch signaling in the immune system. Immunity 2010;32:14-27.
44. Li J, Gordon J, Chen ELY, Xiao S, Wu L, Carlos J, et al. NOTCH1 signaling establishes the medullary thymic epithelial cell progenitor pool during mouse fetal development. The Company of Biologists; 2020. Available at: https://dev.biologists.org/content/develop/147/12/dev178988.full.pdf?with-ds=yes. Accessed July 7, 2020.
45. Liu D, Kousa AI, O'Neill KE, Rouse P, Popis M, Farley AM, et al. Canonical Notch signaling controls the early thymic epithelial progenitor cell state and emergence of the medullary epithelial lineage in fetal thymus development. Development 2020;147:dev178582.
46. Park J-E, Botting RA, Conde CD, Popescu D-M, Lavaert M, Kunz DJ, et al. A cell atlas of human thymic development defines T cell repertoire formation. Science 2020;367:eaay3224.
47. Yui MA, Rothenberg EV. Developmental gene networks: a triathlon on the course to T cell identity. Nat Rev Immunol 2014;14:529-45.
48. Pabst R. The thymus is relevant in the migration of mature lymphocytes. Cell Tissue Res 2019;376:19-24.
49. Rodewald H-R. Thymus organogenesis. Annu Rev Immunol 2008;26:355-88.
50. Abramson J, Anderson G. Thymic epithelial cells. Annu Rev Immunol 2017;35:85-118.
51. Kollmann TR, Goldstein MM, Goldstein H. The concurrent maturation of mouse and human thymocytes in human fetal thymus implanted in NIH-beige-nude-xid mice is associated with the reconstitution of the murine immune system. J Exp Med 1993;177:821-32.
52. Pantelouris EM. Absence of thymus in a mouse mutant. Nature 1968;217:370-1.
53. Kernfeld EM, Genga RMJ, Neherin K, Magaletta ME, Xu P. a single-cell transcriptomic atlas of thymus organogenesis resolves cell types and developmental maturation. Immunity 2018;48:1258-70.e6.
54. Miller CN, Proekt I, Von Moltke J, Wells KL, Rajpurkar AR, Wang H, et al. Thymic tuft cells promote an IL-4-enriched medulla and shape thymocyte development. Nature 2018;559:627-31.
55. Bornstein C, Nevo S, Giladi A, Kadouri N, Pouzolles M, Gerbe F, et al. Single-cell mapping of the thymic stroma identifies IL-25-producing tuft epithelial cells. Nature 2018;559:622-6.

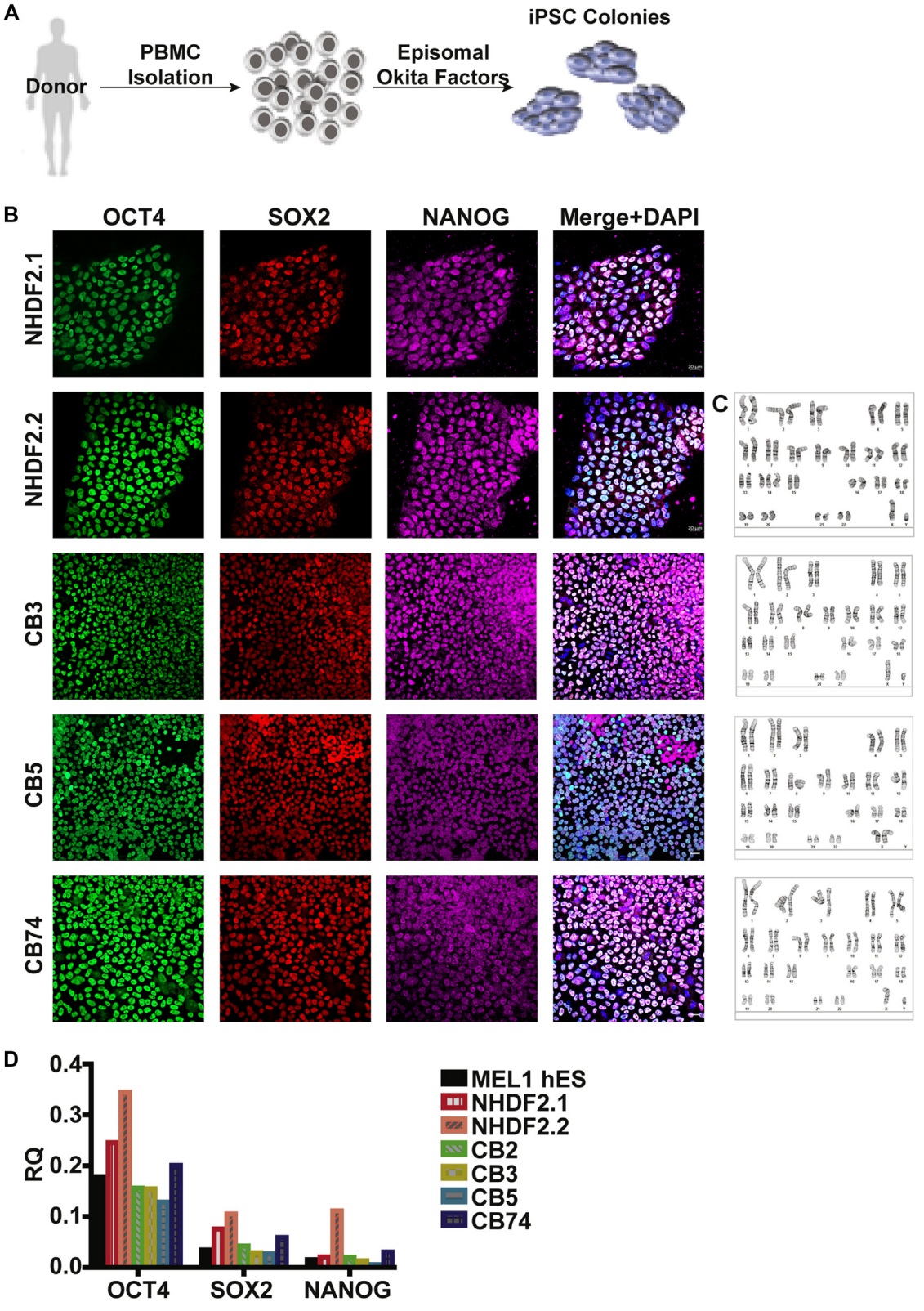

FIG E1. Generation of patient-derived iPSCs from PBMCs. **(A)** Schematic of workflow for reprogramming of PBMCs into patient-derived iPSCs. **(B)** IF analysis of pluripotency marker proteins OCT4 (*green*), SOX2 (*red*), and NANOG (*magenta*). Scale bar = 20 μm. **(C)** Karyotype analysis of established iPSC lines. **(D)** qPCR analysis of pluripotency marker genes *OCT4*, *SOX2*, and *NANOG* in iPSCs. Data are shown as the mean of technical replicates. Values were normalized and set relative to ACTB. Human embryonic stem cells served as positive control.

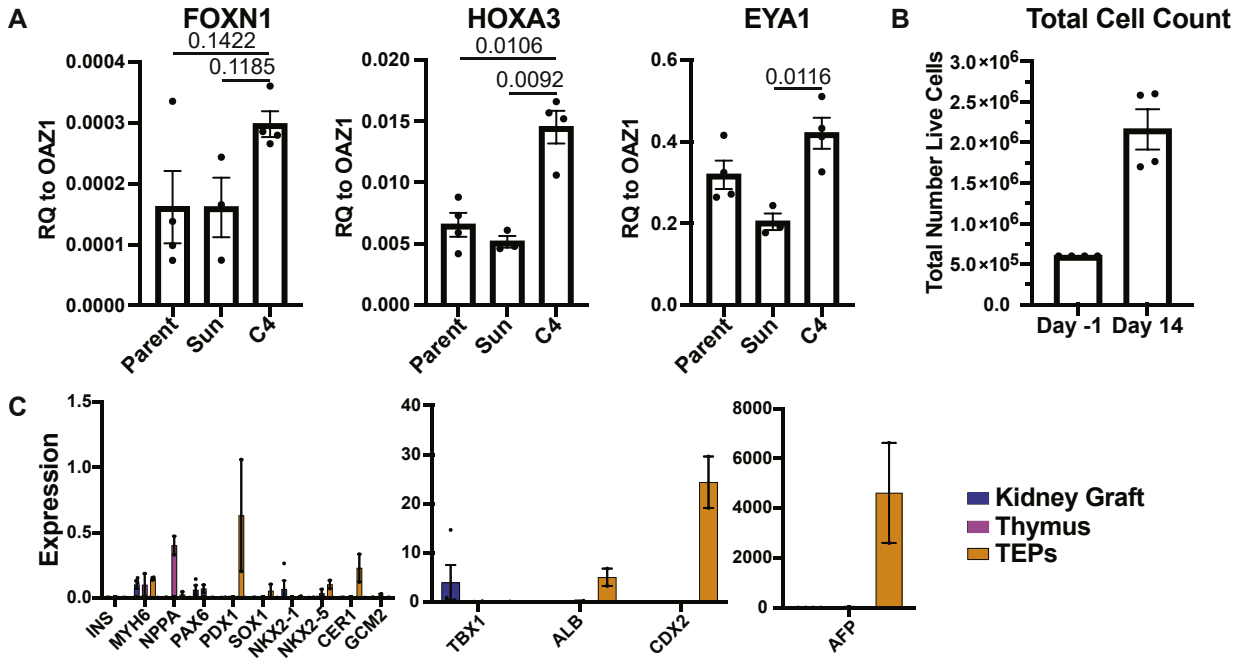

D

	Definitive Endoderm Induction			Third Pharyngeal Pouch Induction	TEP Induction
Day -1	**Day 0**	**Day 1-3**	**Day 4**	**Day 5-8**	**Day 9+**
iPSCs were plated on Matrigel coated plates at 3.15e5 cells/cm^2 in mTeSR Plus, supplemented with 10μM Rock Inhibitor.	24 hours after plating, cells were washed 1x with PBS, and differentiation was induced with XVIVO10 supplemented with 100ng/ml Activin A, 50ng/ml Wnt3a, and ITS(1:5000)	For days 1-3, media was changed daily with XVIVO10 supplemented with Activin A and ITS (1:2000)	On day 4, media was changed to XVIVO10 supplemented with Activin A, 6nM TTNPB, and ITS (1:2000) *should start to see ridges form	For days 5-8, media was changed daily with XVIVO10 supplemented with 20ng/ml BMP4, 6nM TTNPB, 5μM LY364947, and 100ng/ml SAG *Ridges should be more pronounced	For days 9+, media was changed daily with XVIVO10 supplemented with 20ng/ml BMP4, 6nM TTNPB, 5μM LY364947, 50ng/ml Wnt3a, 50ng/ml FGF8b, and 0.25μM SANT-1

FIG E2. Minimal off-target differentiation during direct differentiation of iPSC into TEPs. **(A)** qPCR analysis for expression levels of TPP and TEP markers at d14 of cultures differentiated with previously published protocols compared to condition 4 (n = 4, 2 iPSC lines). **(B)** Quantification of total cell numbers at day −1 and d14 of differentiation employing condition 4. **(C)** Differential gene expression of markers indicative of other undesired cell types of TEP kidney grafts, primary neonatal thymus, and d19 iPSC-derived TEPs. **(D)** Detailed protocol for iPSC to TEP differentiation approach using condition 4.

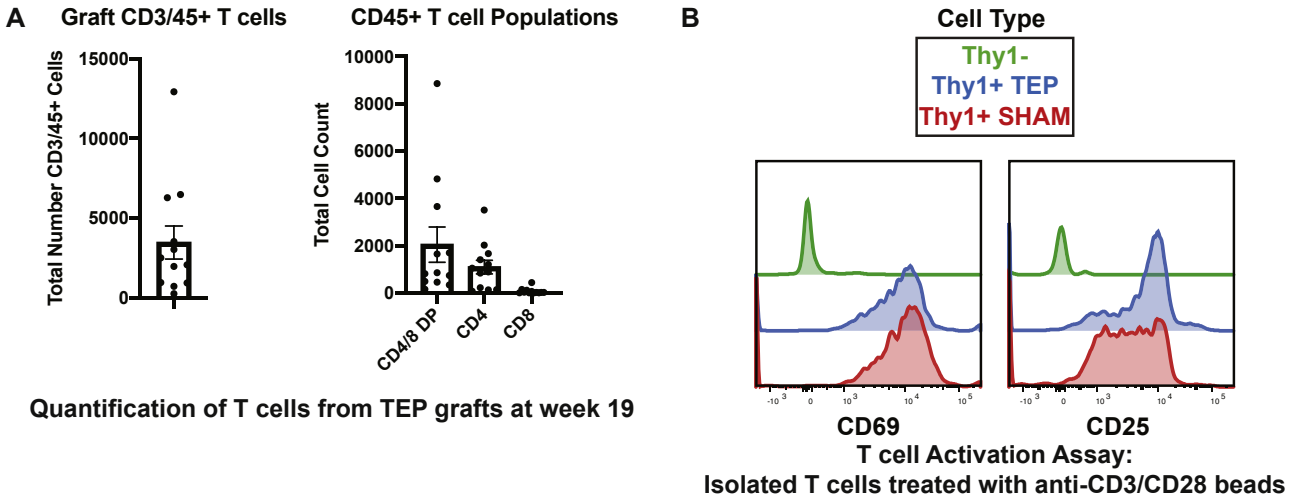

FIG E3. Analysis of mouse T cells in grafts and peripheral T-cell activation *in vitro*. **(A)** Quantification of flow cytometry analysis of different T-cell populations of explanted iPSC-derived TEP grafts (n = 12). **(B)** Representative histograms for activation markers Cd69 or Cd25 of isolated splenocytes from graft-bearing or control mice incubated with Cd3/Cd28 beads *in vitro*. Lineage-negative cells served as additional control (CD25, n = 5 sham, 9 engrafted; CD69, n = 4 sham, 9 engrafted).

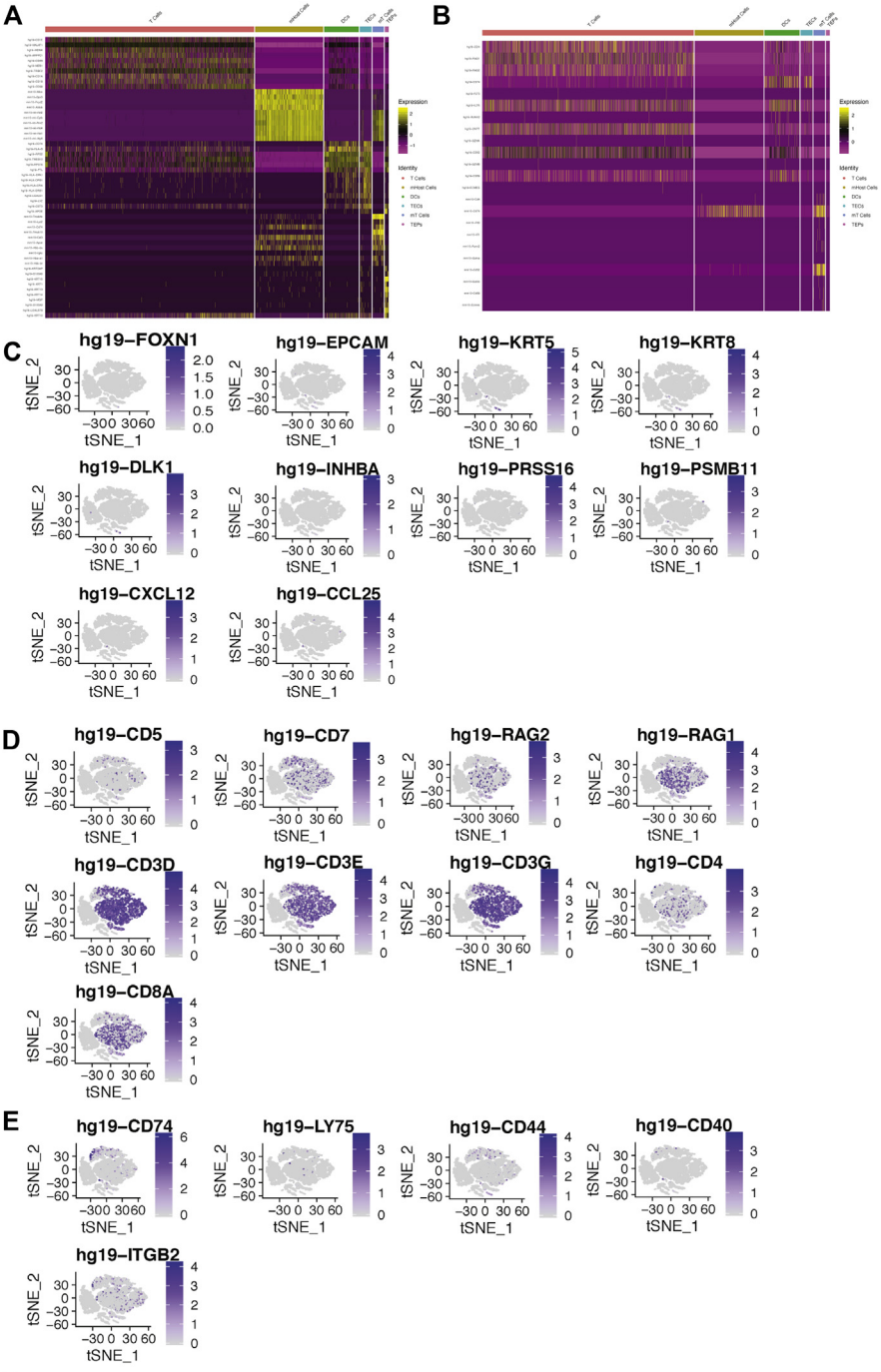

F

Cluster	CB74	NHDF2.2	Thy7.1	Thy7.2
mHost Cells	598 (47.1%)	3062 (80.3%)	0 (0%)	0 (0%)
mT Cells	178 (14.0%)	430 (11.3%)	0 (0%)	2 (4.30E-04%)
T Cells	78 (6.1%)	58 (1.5%)	7413 (87.3%)	3668 (79.2%)
DCs	170 (13.4%)	81 (2.1%)	868 (10.2%)	745 (16.15%)
TEPs	93 (7.3%)	115 (3.0%)	1 (1.20E-04%)	2 (4.30E-04%)
TECs	153 (12.0%)	68 (1.8%)	212 (2.5%)	212 (4.6%)

FIG E4. Single-cell clustering analysis of primary neonatal thymus and grafts. **(A)** Heatmap analysis of top 10 genes expressed in each of the primary clusters. **(B)** Curated heatmap of key marker genes of T-cell development. **(C-E)** Gene-specific tSNEs corresponding to gene-specific violin plots in Fig 4. **(F)** Sample-specific quantification of total cell numbers for each cluster identified in Fig 4, *A*.

A

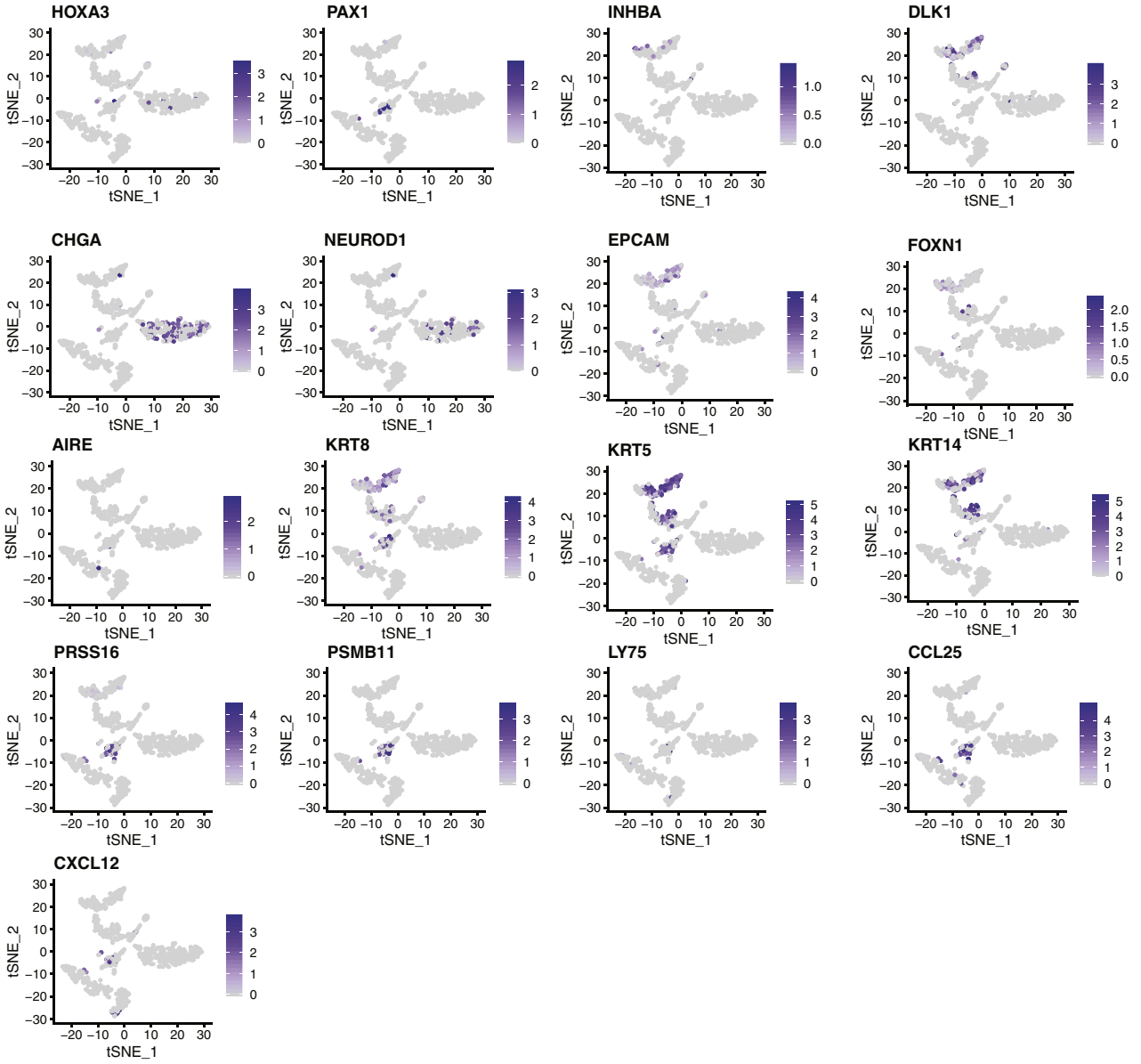

B

Cluster	CB74	NHDF2.2	Thy7.1	Thy7.2
0	67 (27.2%)	31 (16.9%)	63 (29.6%)	89 (41.6%)
1	80 (32.5%)	51 (27.9%)	2 (0.94%)	3 (1.4%)
2	0 (0%)	0 (0%)	69 (32.4%)	53 (24.8%)
3	72 (29.3%)	44 (24.0%)	0 (0%)	0 (0%)
4	24 (9.8%)	7 (3.8%)	14 (6.5%	44 (20.6%)
5	0 (0%)	0 (0%)	45 (21.1%)	8 (3.7%)
6	0 (0%)	0 (0%)	20 (9.4%)	17 (7.9%)
7	1 (0.41%)	30 (16.4%)	0 (0%)	0 (0%)
8	2 (0.81%)	20 (10.9%)	0 (0%)	0 (0%)

FIG E5. Analysis of TEC cluster subclustering. **(A)** Gene-specific tSNE visualization for key thymic markers, corresponding to the gene-specific violin plots in Fig 5. **(B)** Sample-specific quantification of total cell numbers for each cluster identified in Fig 5, *B*.

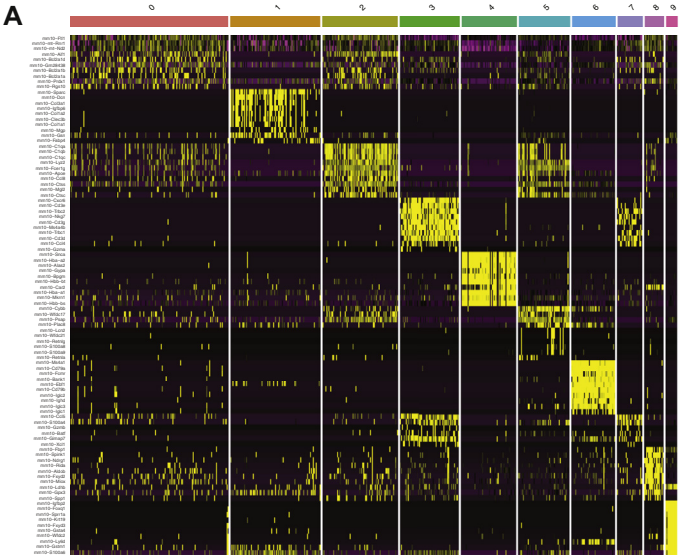

C

Cluster	CB74	NHDF2.2	Thy7.1	Thy7.2
0	21 (11.8%)	141 (32.8%)	0 (0%)	0 (0%)
1	78 (43.8%)	15 (3.5%)	0 (0%)	0 (0%)
2	15 (8.4%)	63 (14.7%)	0 (0%)	0 (0%)
3	3 (1.7%)	59 (13.7%)	0 (0%)	0 (0%)
4	18 (10.1%)	39 (9.1%)	0 (0%)	0 (0%)
5	20 (11.2%)	33 (7.7%)	0 (0%)	0 (0%)
6	10 (5.6%)	35 (8.1%)	0 (0%)	0 (0%)
7	0 (0%)	26 (6.0%)	0 (0%)	0 (0%)
8	1 (0.56%)	19 (4..4%)	0 (0%)	0 (0%)
9	12 (6.7%)	0 (0%)	0 (0%)	0 (0%)

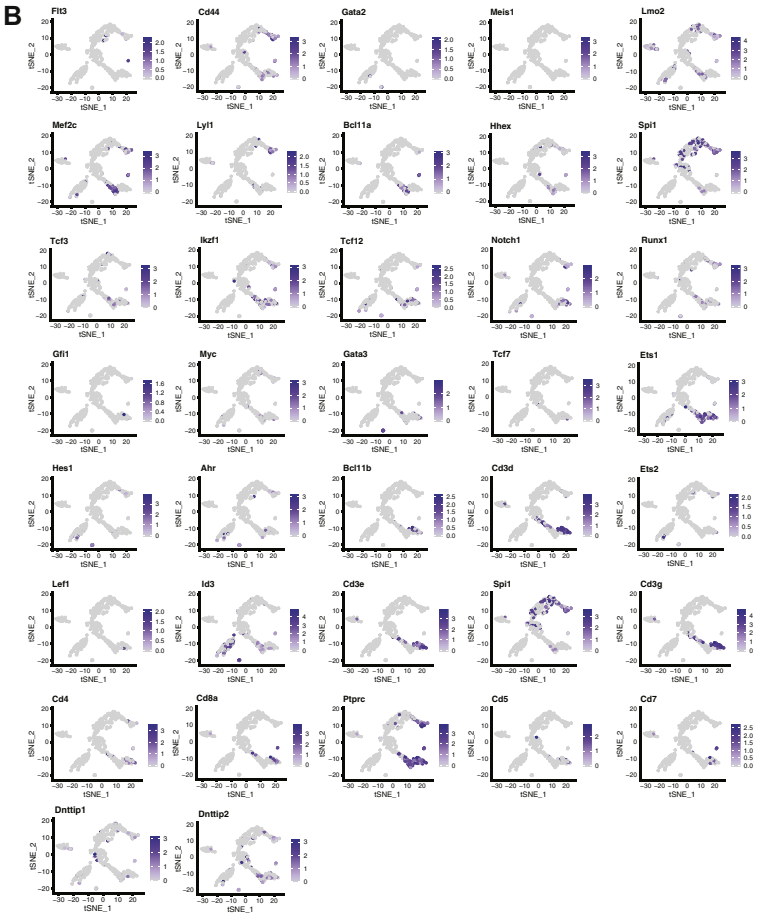

FIG E6. Analysis of mouse-derived cell subclustering. **(A)** Heatmap of the top 10 upregulated genes in each of the mouse T-cell subclusters. **(B)** Gene-specific tSNE visualization of key T-cell markers corresponding to gene-specific violin plots in Fig 6, *F*. **(C)** Sample-specific quantification of total cell numbers for each cluster identified in Fig 6, *B*.